CARDIOLOGY

Desmosomal protein degradation as an underlying cause of arrhythmogenic cardiomyopathy

Hoyee Tsui[1]†, Sebastiaan Johannes van Kampen[1]†, Su Ji Han[1], Viviana Meraviglia[2], Willem B. van Ham[3], Simona Casini[4], Petra van der Kraak[5], Aryan Vink[5], Xiaoke Yin[6], Manuel Mayr[6], Alexandre Bossu[3], Gerard A. Marchal[4], Jantine Monshouwer-Kloots[1], Joep Eding[1], Danielle Versteeg[1], Hesther de Ruiter[1], Karel Bezstarosti[7], Judith Groeneweg[8], Sjoerd J. Klaasen[9], Linda W. van Laake[8], Jeroen A.A. Demmers[7], Geert J.P.L. Kops[9], Christine L. Mummery[2], Toon A.B. van Veen[3], Carol Ann Remme[4], Milena Bellin[2], Eva van Rooij[1,8]*

Arrhythmogenic cardiomyopathy (ACM) is an inherited progressive cardiac disease. Many patients with ACM harbor mutations in desmosomal genes, predominantly in plakophilin-2 (*PKP2*). Although the genetic basis of ACM is well characterized, the underlying disease-driving mechanisms remain unresolved. Explanted hearts from patients with ACM had less PKP2 compared with healthy hearts, which correlated with reduced expression of desmosomal and adherens junction (AJ) proteins. These proteins were also disorganized in areas of fibrotic remodeling. In vitro data from human-induced pluripotent stem cell–derived cardiomyocytes and microtissues carrying the heterozygous *PKP2 c.2013delC* pathogenic mutation also displayed impaired contractility. Knockin mice carrying the equivalent heterozygous *Pkp2 c.1755delA* mutation recapitulated changes in desmosomal and AJ proteins and displayed cardiac dysfunction and fibrosis with age. Global proteomics analysis of 4-month-old heterozygous *Pkp2 c.1755delA* hearts indicated involvement of the ubiquitin-proteasome system (UPS) in ACM pathogenesis. Inhibition of the UPS in mutant mice increased area composita proteins and improved calcium dynamics in isolated cardiomyocytes. Additional proteomics analyses identified lysine ubiquitination sites on the desmosomal proteins, which were more ubiquitinated in mutant mice. In summary, we show that a plakophilin-2 mutation can lead to decreased desmosomal and AJ protein expression through a UPS-dependent mechanism, which preceded cardiac remodeling. These findings suggest that targeting protein degradation and improving desmosomal protein stability may be a potential therapeutic strategy for the treatment of ACM.

INTRODUCTION

Arrhythmogenic cardiomyopathy (ACM) is a progressive, genetic cardiac disease with a prevalence of 1:2000 to 1:5000 (*1*). Diagnosis of ACM remains challenging because of complex clinical presentation and varying disease penetrance (*2*). The clinically concealed phase of ACM commonly progresses in an asymptomatic manner, although patients have a higher susceptibility to sudden cardiac death. With disease progression, an increase in fibrosis and fatty tissue replacement is evident within the myocardium, consequently exacerbating life-threatening ventricular arrhythmias (*3*).

About 50% of patients diagnosed with ACM carry mutations in the desmosomal genes: plakophilin-2 (*PKP2*), plakoglobin (*JUP*), desmoplakin (*DSP*), desmoglein (*DSG*), and desmocollin (*DSC*), with *PKP2* as the most frequently mutated gene (*1*, *3*–*7*). In the heart, desmosomes reside at the short axis of cardiomyocytes in structures termed intercalated discs (IDs), where they facilitate the linkage between adjacent cells. More recently, it has become apparent that desmosomal components can interact with other ID macromolecular structures including numerous ion channels (*6*, *8*–*12*). They also interact with adherens junction (AJ) proteins to generate a hybrid structure known as the area composita (*6*, *8*–*12*). Moreover, several ID components function as scaffolding and signaling molecules, thereby affecting pathways implicated in ACM pathogenesis, such as the Wnt and Hippo signaling pathway (*13*–*16*). In addition, studies conducted on tamoxifen-induced cardiomyocyte-specific deletion of *Pkp2* in adult mice demonstrated disruption of intracellular calcium homeostasis (*17*–*19*). Several studies have noted a decline of desmosomal proteins in cardiac tissue of patients with ACM (*10*, *13*, *20*–*25*), and electron microscopy showed that reduced desmosomal protein correlated with focal widening of the intercellular space at IDs, smaller IDs, and a decrease in the quantity and average length of gap junctions in patients with ACM (*10*, *24*–*27*). Despite these observations, a mechanistic explanation for the role of desmosomal proteins in ACM pathology is still lacking.

Protein degradation is vital for the removal of misfolded and damaged proteins to prevent proteotoxicity. Pathways responsible for proteome homeostasis include the ubiquitin-proteasome system (UPS), the autophagy-lysosome pathway, and pathways involving calcium-dependent calpain and cathepsin proteases (*28*).

[1]Hubrecht Institute, Royal Netherlands Academy of Arts and Sciences (KNAW) and University Medical Center Utrecht, 3584 CT, Netherlands. [2]Department of Anatomy and Embryology, University Medical Center, Leiden, 2333 ZA, Netherlands. [3]Department of Medical Physiology, University Medical Center Utrecht, 3584 CM, Netherlands. [4]Department of Clinical and Experimental Cardiology, University Medical Center Amsterdam, 1105 AZ, Netherlands. [5]Department of Pathology, University Medical Center Utrecht, 3584 CX, Netherlands. [6]James Black Centre, King's College, University of London, WC2R 2LS London, UK. [7]Proteomics Center, Erasmus Medical Center Rotterdam, 3015 CN, Netherlands. [8]Department of Cardiology, University Medical Center Utrecht, 3584 CX, Netherlands. [9]Oncode Institute, Hubrecht Institute, Royal Academy of Arts and Sciences (KNAW) and University Medical Center Utrecht, 3584 CT, Netherlands.
*Corresponding author. Email: e.vanrooij@hubrecht.eu
†These authors contributed equally to this work.

Earlier studies revealed increased instability of mutant PKP2 protein (*PKP2 c.2386T>C* mutation) and mutant DSP protein (*DSP c.1596C>G*), both demonstrating increased sensitivity toward calcium-dependent calpain proteases (*29*, *30*). A recent study uncovered the involvement of subunit 6 of the constitutive photomorphogenesis 9 signalosome (CSN6) in ACM through prevention of neddylation-directed proteome degradation (*31*). These studies highlight the importance of protein degradation pathways in ACM pathogenesis and the importance of fully functioning desmosomes in cardiac physiology.

Here, we show that hallmarks observed in patients with ACM are recapitulated in human-induced pluripotent stem cell–derived cardiomyocytes (hiPSC-CMs) and microtissues (MTs; both bearing the *PKP2 c.2013delC* mutation) and in heterozygous *Pkp2 c.1755delA* knockin mice (equivalent to the human *PKP2 c.2013delC* mutation). The effects on protein degradation in mutant mice were rescued by UPS inhibition, which also translated into functional improvement, because calcium dysregulation was restored in cardiomyocytes. Ubiquitin proteomics analysis demonstrated increased protein ubiquitination in mutant mouse hearts when compared with those of wild-type (WT) littermates and identified the specific ubiquitination site on PKP2 as well as on other desmosomal and AJ proteins. These data suggest that the UPS may be involved in ACM pathogenesis and open up new avenues for therapeutic development to restore PKP2 and desmosome integrity in these patients.

RESULTS

Pathological remodeling in patients with ACM coincides with desmosomal protein decline

To study pathological features of ACM, we collected explanted heart tissue from healthy controls and patients with ACM bearing mutations in the *PKP2* gene (Table 1). All *PKP2* mutation–bearing patients initially presented with ACM symptoms, which had developed into biventricular heart failure at the time of heart transplantation (Table 1). Compared with controls, Masson's trichrome staining of patient cardiac tissue demonstrated typical hallmarks of ACM regardless of which mutation was present, including increased cardiomyocyte disarrangement, fibrosis, and fibrofatty replacement (Fig. 1A and fig. S1, A and B) (*2*). Immunostaining for desmosomal proteins showed a misalignment of PKP2, JUP, and DSP proteins within the myocardium. This occurred in both ventricles and was most pronounced at sites with extensive fibrosis (Fig. 1, B to D; and fig. S1, C to E). Immunoblot analysis confirmed the biventricular decrease in desmosomal proteins in patients with ACM harboring *PKP2* mutations (Fig. 1, E and F, and fig. S1F). Misalignment of desmosomes was also observed in other ACM hearts bearing different *PKP2* mutations (figs. S2 to S4).

To determine the extent of desmosomal protein decline for other disease-driving mutations, we performed immunoblots on patient samples bearing mutations in *DSP* (*c.1705A>T*) or phospholamban (*PLN c.40-42delAGA*). Within the four *PLN* mutation carriers, two were diagnosed with ACM and dilated cardiomyopathy (DCM), and two were diagnosed with only DCM (Table 1). The loss in desmosomal proteins was recapitulated in two *PLN* carriers; one was diagnosed with ACM and DCM, and the other was diagnosed with only DCM (Fig. 1E, Table 1, and fig. S1F). Subsequent correlation analysis indicated a strong positive relationship between PKP2 protein expression and other desmosomal proteins (Fig. 1, G to J). Our data suggest that the decline in desmosomal protein expression may be more prevalent in patients with ACM bearing a *PKP2* mutation, but more patient samples will be required to confirm this relationship in patients with DCM or ACM bearing other mutations.

Pathogenic *PKP2* mutant hiPSC-CMs demonstrate functional deficiency

To further interrogate the pathomolecular changes, we used hiPSC-CMs derived from a patient harboring the *PKP2 c.2013delC* mutation ($PKP2^{c.2013delC/WT}$) and used CRISPR-Cas9 to generate the corresponding isogenic control line (figs. S5 and S6A) (*32*, *33*). In support of our observations in cardiac tissue from patients with ACM, $PKP2^{c.2013delC/WT}$ hiPSC-CMs demonstrated a reduction in PKP2 protein and mRNA expression, whereas the other desmosomal components only displayed a reduction in protein expression; this occurred without apparent changes in cellular localization compared with isogenic control (fig. S6, B to K). This was confirmed by bulk RNA sequencing on $PKP2^{c.2013delC/WT}$ and control hiPSC-CMs, which revealed that only a small number of reads originated from the mutant allele (fig. S6L). Previous studies have shown that PKP2 insufficiency can lead to a sodium current deficit (*34*, *35*). Therefore, we examined whether this functional effect would be evident in our $PKP2^{c.2013delC/WT}$ hiPSC-CMs. Here, we also observed a decreased sodium current (I_{Na}) density [current (picoampere) normalized to cell membrane capacitance (picofarad), picoampere/picofarad] in $PKP2^{c.2013delC/WT}$ hiPSC-CMs compared with isogenic controls (fig. S6, M to O, and table S1). This reduction might decrease the action potential upstroke velocity, which, in turn, can lead to slower conduction (*35*). The I_{Na} voltage dependence of activation and inactivation, assessed as the half voltage of (in)activation ($V_{1/2}$) and the slope factor k, were similar in both groups.

To examine the role of PKP2 in cell-cell adhesion among different cell types, we generated and characterized cardiac MTs bearing the heterozygous *PKP2 c.2013delC* mutation in cardiomyocytes. MTs were composed of 70% hiPSC-CMs, 15% hiPSC–cardiac fibroblasts (hiPSC-CFs), and 15% hiPSC–endothelial cells (hiPSC-ECs) (Fig. 2A) (*36*, *37*). Compared with isogenic control MTs, $PKP2^{c.2013delC/WT}$ MTs demonstrated reduced PKP2 protein by immunostaining, similar to hiPSC-CMs and cardiac tissue from patients with ACM (Fig. 2B). We also found that the $PKP2^{c.2013delC/WT}$ MTs had a significantly ($P < 0.0001$) reduced ability to respond to increased pacing under high stimulation frequencies (>2 Hz), resulting in arrhythmic behavior (Fig. 2, C and D). Together, these data show that a single point mutation in *PKP2* was associated with a loss in PKP2 and desmosomal proteins, which corresponded with contractile and electrical dysfunction in mutant cardiomyocytes.

Mice carrying a human pathogenic *PKP2* mutation show cardiac dysfunction and remodeling

To study the in vivo relevance of this *PKP2* mutation, we used CRISPR-Cas9 to knock in the mouse equivalent of the human pathogenic *PKP2 c.2013delC* mutation (*Pkp2 c.1755delA*) (fig. S7). Two-month-old $Pkp2^{c.1755delA/WT}$ mice demonstrated a significant decrease in PKP2 mRNA and protein ($P < 0.001$ and $P < 0.01$, respectively), whereas immunohistochemistry data indicated that this did

Table 1. Clinical data of the explanted hearts from patients. ACM, arrhythmogenic cardiomyopathy; BiVAD, biventricular assist device; DCM, dilated cardiomyopathy; *DSP*, desmoplakin; ECG, electrocardiogram; F, female; LVAD, left VAD; M, male; MCS, mechanical circulatory support; *PKP2*, plakophilin-2; *PLN*, phospholamban; QRS, electrocardiographic complex consisting of the Q, R, and S wave; RVAD, right VAD; SR, sinus rhythm; VF, ventricular fibrillation; VT, ventricular tachycardia.

Gene mutation	Protein change	Sex	Age at transplant	Initial clinical diagnosis	End-stage heart failure	ECG	Sustained ventricular arrhythmias	MCS before transplant
PKP2 c.235C>T	p.Arg79X	M	61	ACM	Yes	•SR •Left axis •Interventricular conduction delay	VT	None
PKP2 c.2386T>C	p.Cys796Arg	F	56	ACM	Yes	•SR •Microvoltages •Negative T waves V1–V6	VT	None
PKP2 c.397C>T	p.Gln133X	M	66	ACM	Yes	•SR •Microvoltages •Negative T waves V1–V4 •Ventricular extrasystoles	VF	None
PKP2 c.2544G>A	p.Trp848X	M	47	ACM	Yes	•Atrial pacing •Interventricular conduction delay •Microvoltages •Negative T waves V1–V5	VT	None
DSP c.1705A>T	p.Lys569X	M	44	DCM	Yes	•SR •Microvoltages •Delayed terminal activation •Negative T waves V4–V6	None	None
PLN c.40-42delAGA	p.Arg14del	F	55	ACM and DCM	Yes	•SR •Left axis •QS pattern precordially •Ventricular extrasystoles	VT	LVAD, temporary RVAD
PLN c.40-42delAGA	p.Arg14del	M	72	DCM	Yes	•SR •Microvoltages •Ventricular extrasystoles	None	LVAD
PLN c.40-42delAGA	p.Arg14del	F	37	ACM & DCM	Yes	•SR •Microvoltages (QRS < *P*)	VF	BiVAD
PLN c.40-42delAGA	p.Arg14del	F	58	DCM	Yes	•SR •Microvoltages •Ventricular extrasystoles	None	LVAD

not affect PKP2 localization (Fig. 3, A to D). Similar to the hiPSC-CMs, bulk RNA sequencing data showed virtually nondetectable mutant allelic reads in the $Pkp2^{c.1755delA/WT}$ heart samples, suggesting that it is largely the WT mRNA that is expressed (fig. S8A). In addition, apart from *Pkp2* mRNA decline, there was a lack of mRNA changes for the other desmosomal components at 2 months of age in $Pkp2^{c.1755delA/WT}$ heart samples, which corroborates the data from hiPSC-CMs (fig. S8, B and C). However, with age (12 months old), *Jup* and *Dsp* mRNA expressions were decreased (fig. S8, D and E).

Although functional and histological analysis in 2-month-old $Pkp2^{c.1755delA/WT}$ mouse hearts did not show an overt phenotype, progressive signs of ACM became evident with age (table S2). In 12-month-old $Pkp2^{c.1755delA/WT}$ mice, there was a decrease in early/late (E/A) ratio, a measure of ventricular refilling efficiency between contractions (Fig. 3E), and an increase in isovolumic

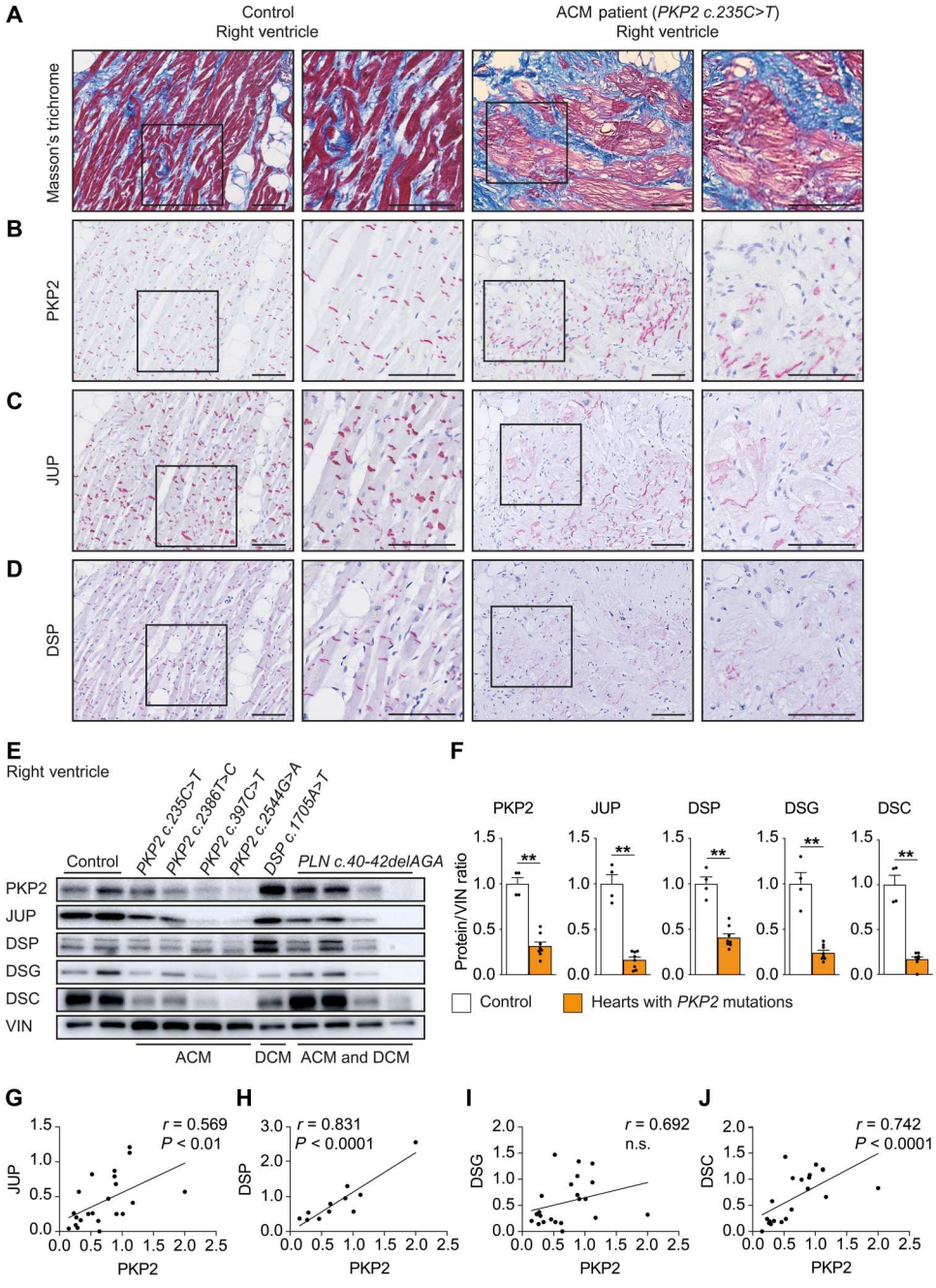

Fig. 1. Explanted ACM human hearts display desmosomal disorganization in areas of fibrofatty remodeling. (**A** to **E**) Right ventricular samples. (A) Masson's trichrome staining, highlighting muscle cells (red), fibrotic regions (blue), and adipocytes (white); immunostaining for PKP2 (B), JUP (C), and DSP (D) from an explanted control and ACM heart (*PKP2 c.235C>T*). Insets represent a close-up of an extensively remodeled region. Protein of interest is stained in red, and nuclei are counterstained in blue. Scale bars, 100 μm. (E) Protein expression of desmosomal components was assessed by Western blot from explanted control hearts ($n = 2$) and hearts obtained from patients carrying the indicated mutations in *PKP2* ($n = 4$), *DSP* ($n = 1$), or *PLN* ($n = 4$). (**F**) Quantification of desmosomal proteins relative to VIN (vinculin) in right and left ventricular biopsies obtained from control hearts ($n = 2$) and ACM human hearts with a mutation in *PKP2* ($n = 4$). (**G** to **J**) Correlation between the protein abundance, based on immunoblot analysis (F) and fig. S1F, of PKP2 and JUP (G), DSP (H), DSG (I), and DSC (J) in left and right ventricular tissue of explanted control hearts ($n = 2$) and from hearts obtained from patients carrying mutations in *PKP2* ($n = 4$), *DSP* ($n = 1$), or *PLN* ($n = 4$). Correlation and significance were assessed by nonparametric Spearman correlation (two-tailed, 95% confidence interval). For each panel, the correlation coefficient (r) and P value are shown. Protein expression data (F) were plotted as means ± SEM. Significance has been assessed by a two-tailed Mann-Whitney test (**$P < 0.01$). n.s., not significant.

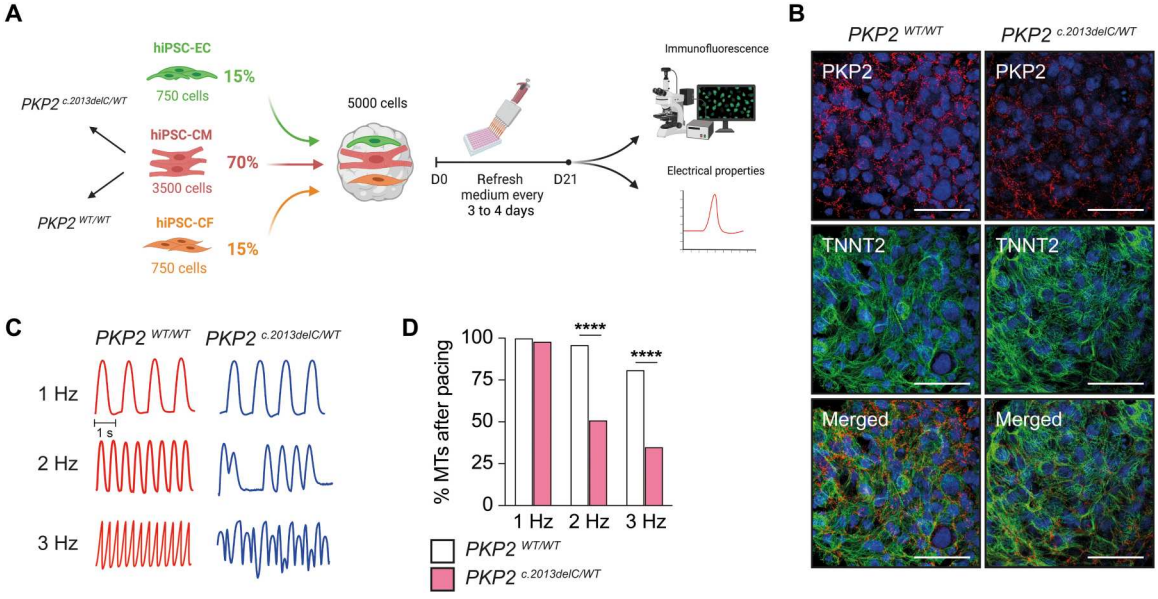

Fig. 2. Cardiac MTs containing heterozygous *PKP2 c.2013delC* hiPSC-CMs show impaired contractility. (**A**) Schematic showing cardiac microtissue (MT) formation. The MTs contain 70% of hiPSC-derived cardiomyocytes ($PKP2^{c2013delC/WT}$ hiPSC-CMs), 15% of endothelial cells ($PKP2^{WT/WT}$ hiPSC-ECs), and 15% of cardiac fibroblasts ($PKP2^{WT/WT}$ hiPSC-CFs). (**B**) Immunofluorescence staining of PKP2 (red), cardiac troponin-T (TNNT2, green), and 4′,6-diamidino-2-phenylindole (DAPI; blue) in $PKP2^{c.2013delC/WT}$ or control MTs. Scale bars, 50 μm. (**C**) Representative contraction traces from control and mutant MTs stimulated at 1, 2, and 3 Hz. (**D**) Percentages of paced MTs that were able to respond at different stimulation frequencies (n = 55 to 57 MTs per group and n = 5 independent MT batches coming from different experiments of MT formation). Chi-square test was used to assess significance (****P < 0.0001).

relaxation time (IVRT) (Fig. 3F), both possible signs of impaired ventricular relaxation. The T wave in an electrocardiogram is also indicative of ventricular relaxation and diastolic function. T wave abnormalities are commonly seen in patients with ACM and are also evident in our clinical data (Table 1) (*2*, *38*, *39*). However, ejection fraction (EF), a measure for systolic function and left ventricular contractility, remained comparable between groups (Fig. 3G). Sirius red staining indicated an increase in interstitial cardiac fibrosis in 12-month-old $Pkp2^{c.1755delA/WT}$ mice when compared with WT littermates, which was corroborated by an increase in total cardiac collagen abundance in mutant mice, as measured by hydroxyproline content (Fig. 3, H and I, and fig. S8F). Immunohistochemistry in $Pkp2^{c.1755delA/WT}$ mouse hearts for PKP2, JUP, and DSP also revealed desmosomal disorganization in fibrotic regions, as seen by increased ID width that was absent in WT and nonfibrotic regions of $Pkp2^{c.1755delA/WT}$ hearts (Fig. 3, J and K).

Together, these data indicate that the human pathogenic mutation in mice induces *Pkp2* haploinsufficiency. Subsequent fibrosis and desmosomal protein disorganization in regions of remodeling were observed alongside cardiac stiffening and dysfunction. These observations corroborate the clinical findings in patients with ACM where disorganization of desmosomal proteins was evident in regions of pathological fibrotic remodeling.

Cardiac desmosomal and AJ proteins are reduced in $Pkp2^{c.1755delA/WT}$ mice

To explore the mechanism underlying the pathogenic *Pkp2* mutation, we performed proteomics analysis on 4-month-old heart lysates of $Pkp2^{c.1755delA/WT}$ mice and WT littermates. This revealed a significant up-regulation of 114 proteins and a down-regulation of 31 proteins when compared with WT littermates (fold change of >1.25 or <0.8 and a P value of <0.05; Fig. 4A and table S3). In addition to PKP2, JUP, DSP, and DSG were decreased in $Pkp2^{c.1755delA/WT}$ mouse hearts compared with control hearts (Fig. 4, A and B), which was further confirmed by immunoblots (Fig. 4, C and D). Although DSC changes were not detected in the proteomics data, immunoblots showed a decline in DSC in $Pkp2^{c.1755delA/WT}$ mice (Fig. 4, C and D). The observed decrease in desmosomal proteins from $Pkp2^{c.1755delA/WT}$ mice is likely regulated posttranslationally, because mRNA expression was unchanged at this time point (fig. S8B).

Along with desmosomal proteins, AJ proteins are important for the maintenance of cell-to-cell adhesion between cardiomyocytes via the area composita (*6*, *9*, *12*). Proteomics analysis also identified a decline in several AJ proteins, such as β-catenin (β-CAT), N-cadherin (N-CAD), and α-CAT (Fig. 4, A and B), which was validated by immunoblots (Fig. 4, E and F). Other ACM-related proteins, such as four and a half LIM domain 1 and LIM domain binding 3 (*40*–*44*), were also decreased in $Pkp2^{c.1755delA/WT}$ mice compared with controls (Fig. 4, B, G, and H).

The reduction in desmosomal proteins was consistently demonstrated in 12-month-old $Pkp2^{c.1755delA/WT}$ mice compared with WT littermates (Fig. 5, A and B). At this time point, *Jup* and *Dsp* mRNA expressions were also reduced (fig. S8D). Immunoblot analysis also showed sustained reduction in the AJ proteins β-CAT, N-CAD, and α-CAT in $Pkp2^{c.1755delA/WT}$ mice hearts when compared with controls (Fig. 5, C and D). In addition, immunofluorescent labeling in $Pkp2^{c.1755delA/WT}$ mice demonstrated that disorganization of AJ proteins was evident in severe fibrotic regions of the myocardium (Fig. 5, E and F).

Our data show that a heterozygous point mutation in *Pkp2* leads to decreased expression of ACM-related proteins. These molecular

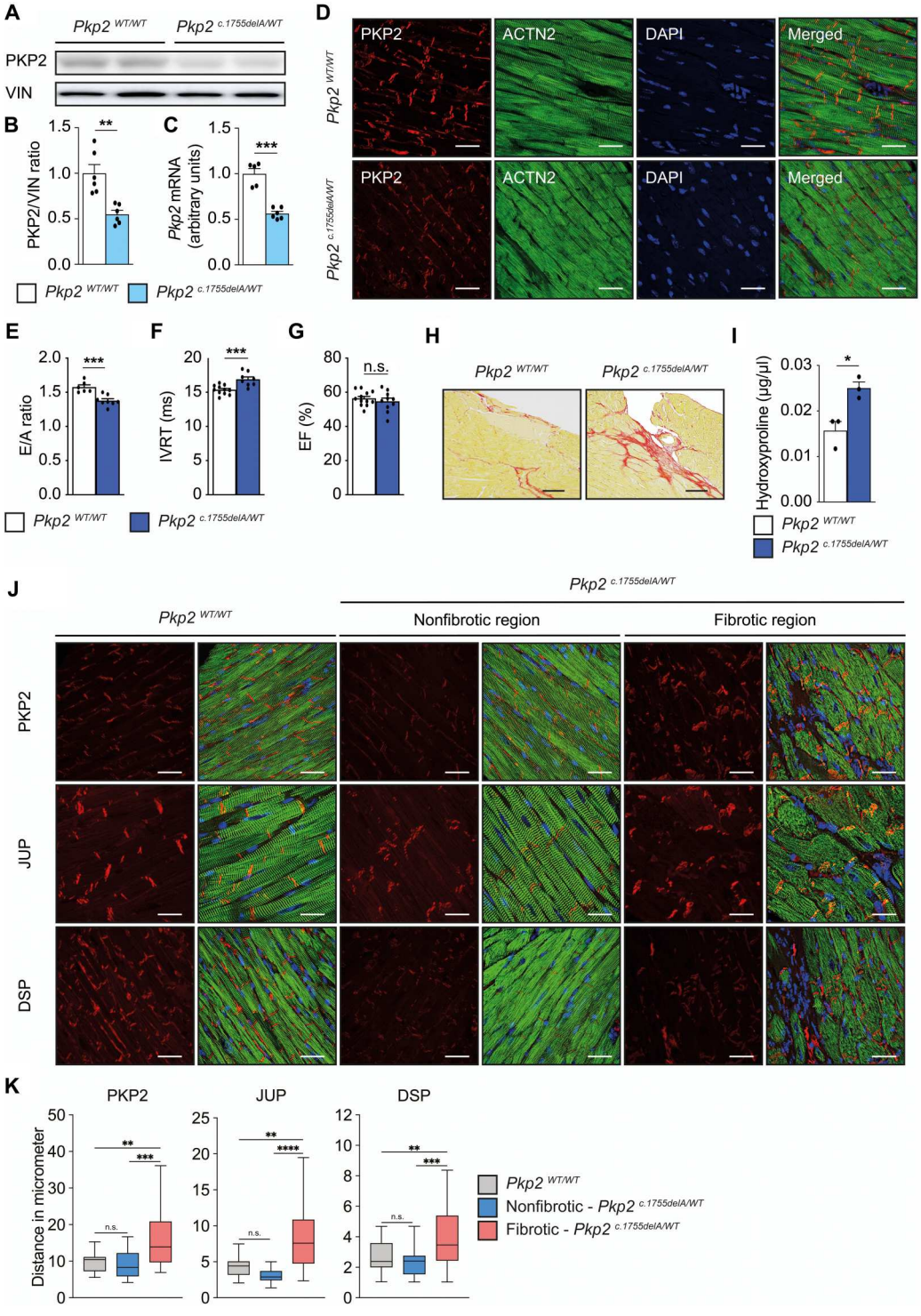

Fig. 3. *Pkp2*$^{c.1755delA/WT}$ mice at 12-months display disorganized IDs under baseline conditions. (**A** to **D**) Molecular analyses on ventricular tissue from 8-week-old mice. (A and B) Immunoblot (A) and quantification of PKP2 protein relative to VIN [(B); $n = 6$ per group]. (C) mRNA expression of *Pkp2* ($n = 5$ to 6 per group). Values normalized to *Gapdh*. (D) Representative images of immunofluorescence staining for PKP2 (red) localization in mouse cardiac tissue, α-actinin 2 (ACTN2), green; DAPI, blue. Scale bars, 50 μm. (**E** to **G**) Cardiac function in 12-month-old mice. (E) Ratio of the early "E" and late "A" ventricular filling velocities ($n = 6$ to 8 per group). (F) Isovolumic relaxation time (IVRT) in milliseconds ($n = 8$ to 11 per group). (G) Ejection fraction (EF; $n = 10$ to 12 per group). (**H**) Representative images of Sirius red staining in 12-month-old mouse hearts. Scale bars, 100 μm. (**I**) Hydroxyproline abundance in ventricular tissue ($n = 3$ per group). (**J**) Immunofluorescence staining for PKP2, JUP, and DSP in 12-month-old mouse hearts in nonfibrotic and fibrotic areas (PKP2, JUP, or DSP, red; ACTN2, green; DAPI, blue). Scale bars, 50 μm. (**K**) Width of the ID (μm) was measured on the basis of the presence of PKP2, JUP, and DSP immunostaining ($n = 18$ to 40 measurements from three mice). Data were plotted as means ± SEM. Significance has been assessed by a one-tailed (I) or two-tailed (B, C, and E to G) Mann-Whitney test. For (K), significance was assessed by one-way ANOVA (DSP) or a Kruskal-Wallis test (PKP2 and JUP) when data were not normally distributed (*$P < 0.05$; **$P < 0.01$; ***$P < 0.001$; ****$P < 0.0001$).

changes precede functional and morphological defects observed in older mice, indicating their potential involvement in ACM pathogenesis.

AJ proteins are reduced and disorganized within severely fibrotic regions in hearts from patients with ACM

To extend our findings on AJ proteins in mice to humans, we performed immunohistochemical staining of β-CAT and N-CAD on ACM heart samples bearing different *PKP2* mutations (Fig. 6, A and B; and figs. S9 and S10, A and B). The AJ proteins in regions of fibrotic remodeling were shown to be more dispersed across a

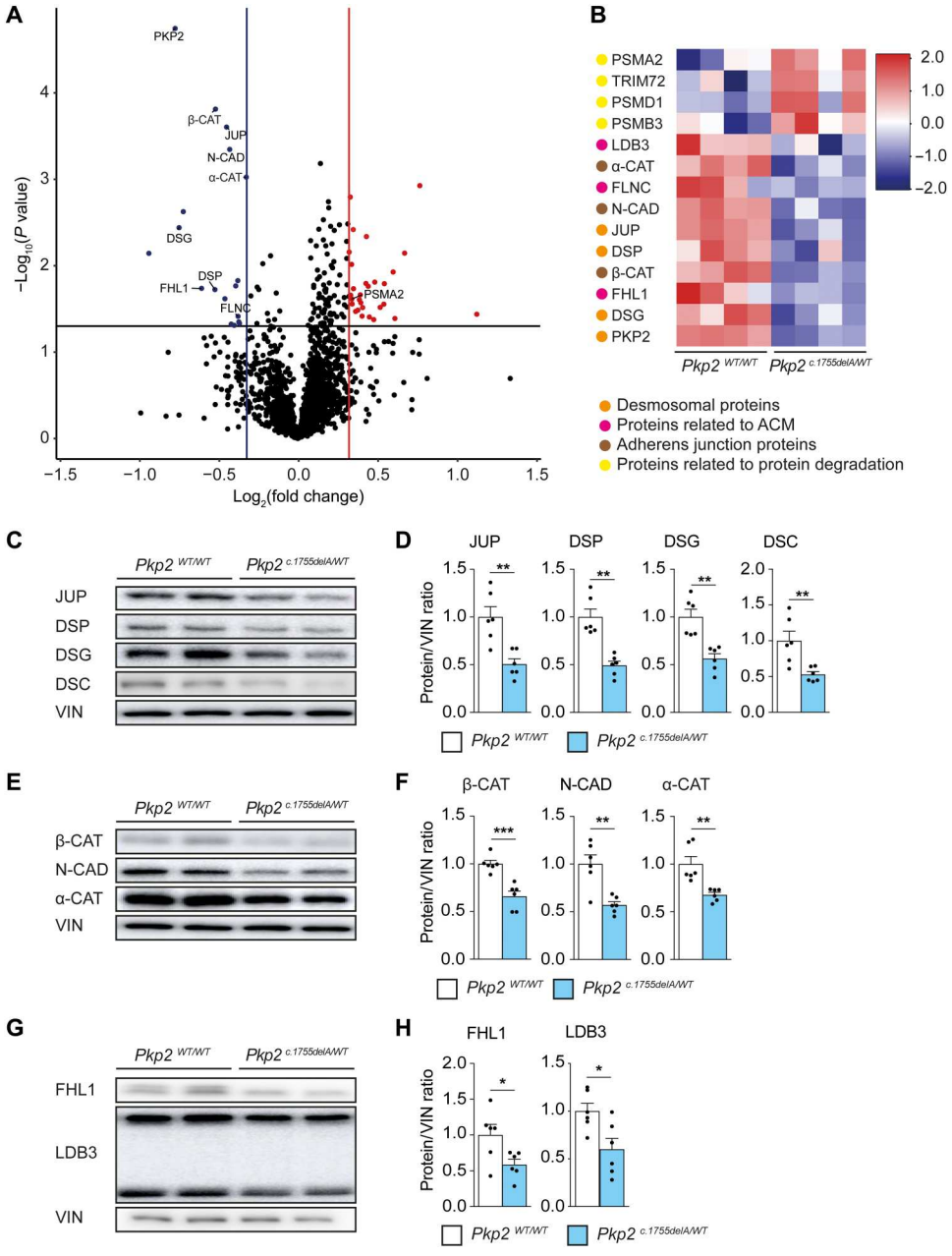

Fig. 4. Proteomics reveals loss of structural and signaling proteins in 4-month-old *Pkp2*$^{c.1755delA/WT}$ mice. (**A** to **H**) Heart tissue from both ventricles was used. (**A**) Volcano plot depicting differentially expressed proteins, comparing 4-month-old *Pkp2*$^{WT/WT}$ and *Pkp2*$^{c.1755delA/WT}$ mice. $n = 4$ mice per group, cutoff of 1.25× up-regulated (red) or 0.8× down-regulated (blue) in *Pkp2*$^{c.1755delA/WT}$ mice, $P < 0.05$. (**B**) Heatmap of differentially expressed desmosomal proteins (orange), proteins previously implicated in ACM pathogenesis (magenta), AJ proteins (brown), and proteins involved in protein degradation (yellow) ($n = 4$ mice per group). Red indicates increased expression in *Pkp2*$^{c.1755delA/WT}$ mice compared with WT. (**C** to **H**) Representative immunoblots ($n = 2$ per group) and the respective protein quantifications for desmosomal (C and D), AJ (E and F), and ACM-linked (G and H) proteins in 8-week-old mice ($n = 6$ per group, VIN as loading control). Protein expression data (D, F, and H) were plotted as means ± SEM. Significance has been assessed by a two-tailed Mann-Whitney test (*$P < 0.05$; **$P < 0.01$; ***$P < 0.001$).

larger region, which corroborated our observations in mice. Furthermore, immunoblots of heart lysates from *PKP2* mutation–bearing patients with ACM demonstrated a prominent biventricular reduction in the AJ proteins, β-CAT, N-CAD, and α-CAT (Fig. 6, C and D, and fig. S10C). Subsequent correlation analysis on heart lysates from patients bearing different mutations in *PKP2*, *DSP c.1705A>T*, or *PLN c.40-42delAGA* indicated that AJ protein expression correlated with PKP2 protein (Fig. 6, C and E to G).

Proteasomal degradation as the underlying cause of protein decline induced by a *Pkp2* mutation in mice

Our in vivo and in vitro findings demonstrated that *PKP2* mutation correlated with the reduction of other desmosomal proteins in the

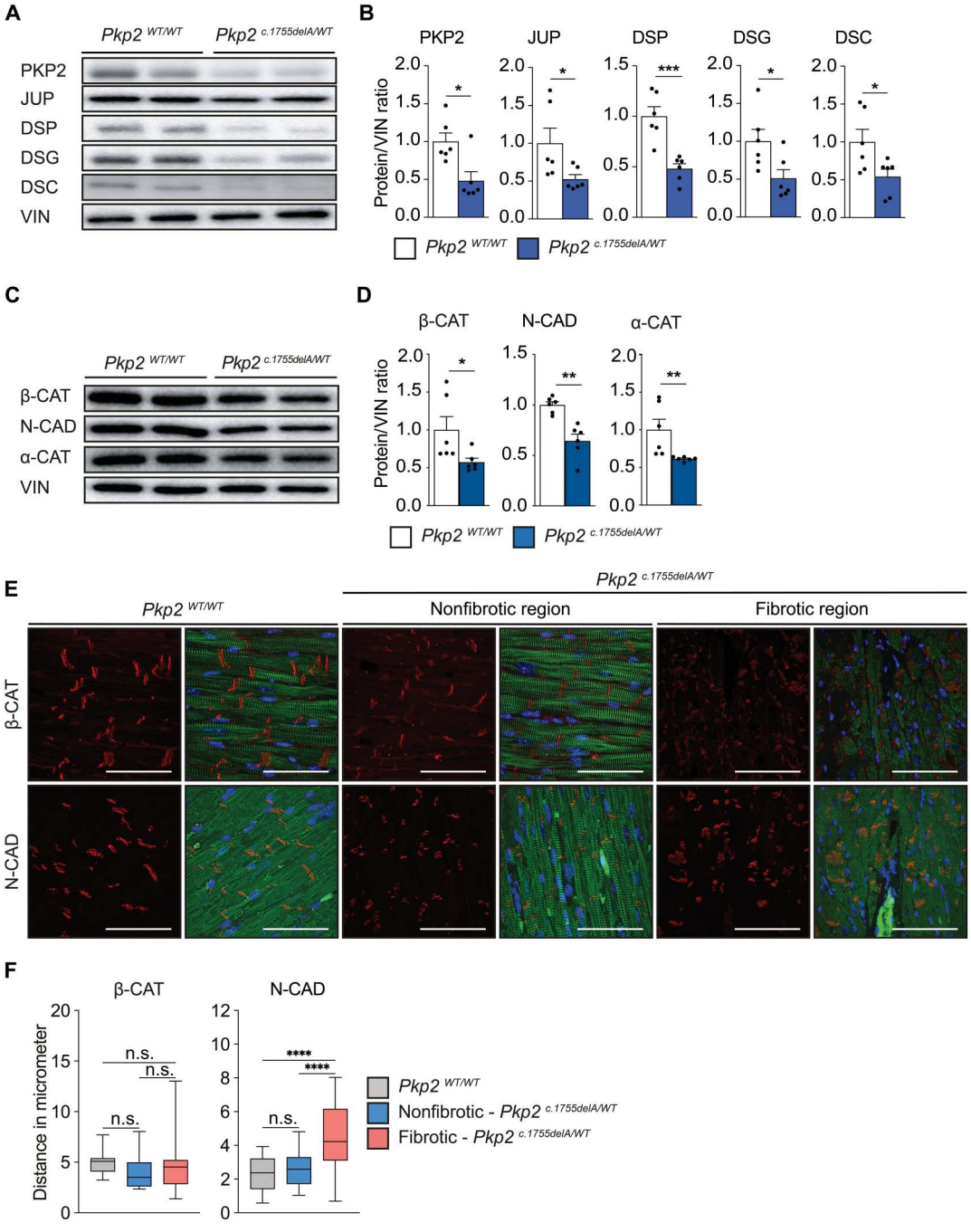

Fig. 5. Desmosomal and AJ proteins are reduced in 12-month-old *Pkp2*$^{c.1755delA/WT}$ mice. (**A** to **F**) Molecular analyses of ventricular tissue from 12-month-old mice. Representative immunoblots (n = 2 per group) and the respective protein quantification of desmosomal (A and B) and AJ (C and D) proteins (n = 6 per group, VIN as loading control). (**E**) Representative immunofluorescence images for β-CAT and N-CAD staining in nonfibrotic and fibrotic areas of mouse hearts (β-CAT and N-CAD in red, ACTN2 in green, and DAPI in blue). Scale bars, 50 μm. (**F**) Width of the ID (micrometer) in 12-month-old mice was measured on the basis of the presence of β-CAT and N-CAD immunostaining (n = 15 to 35 measurements from three mice). Expression data were plotted as means ± SEM. For (B) and (D), significance has been assessed by a two-tailed Mann-Whitney test. For (F), significance was assessed by one-way ANOVA (N-CAD), or a Kruskal-Wallis test (β-CAT) was performed when data were not normally distributed (*P < 0.05; **P < 0.01; ***P < 0.001; ****P < 0.0001).

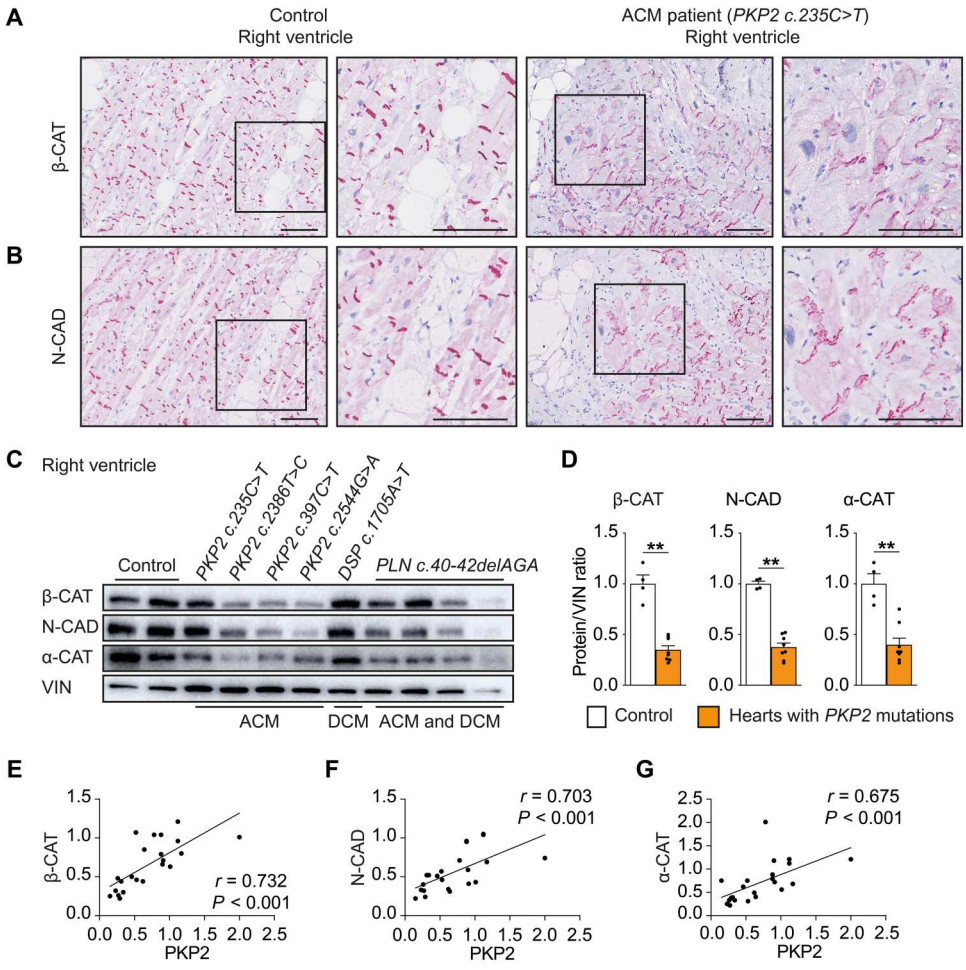

Fig. 6. Reduced expression and disorganization of AJ proteins in areas of extensive remodeling in explanted human ACM hearts. (**A** to **C**) Samples were collected from right ventricles. Representative immunostaining for β-CAT (A) and N-CAD (B) from a control and ACM heart (*PKP2 c.235C>T*). Insets represent a close-up of an extensively remodeled region. Scale bars, 100 μm. (C) Immunoblots for AJ components in tissue from explanted control hearts ($n = 2$) and hearts obtained from patients carrying the indicated mutations: *PKP2* ($n = 4$), *DSP* ($n = 1$), or *PLN* ($n = 4$). (**D**) Quantification of AJ proteins relative to VIN in cardiac tissue obtained from the right and left ventricles of ACM hearts bearing a *PKP2* mutation. (**E** to **G**) Correlation between the protein abundance of PKP2 and β-CAT (E), N-CAD (F), and α-CAT (G) in left and right ventricular tissue of explanted control hearts ($n = 2$) and from hearts with the indicated mutations; calculated from immunoblots in (C) and fig. S10C. Correlation and significance have been assessed by nonparametric Spearman correlation (two-tailed, 95% confidence interval). For each panel, the *r* and *P* value are shown. Protein expression data in (D) were plotted as means ± SEM. Significance has been assessed by a two-tailed Mann-Whitney test (**$P < 0.01$).

absence of mRNA changes. In vivo proteomics data also indicated increased expression of protein components from the UPS, PSMA2 (proteasome 20*S* subunit α2), TRIM72 (tripartite motif containing 72 E3 ubiquitin protein ligase), PSMD1 (proteasome 26*S* subunit, non–adenosine triphosphatase 1), and PSMB3 (proteasome 20*S* subunit β3) (Fig. 4, A and B) (*45*). Led by the above findings, we hypothesized that the UPS, at least in part, is involved in the observed reduction of desmosomal proteins caused by a loss in PKP2 protein expression.

As a proof of concept to show UPS involvement, we subjected $Pkp2^{c.1755delA/WT}$ mice and control mice to daily intraperitoneal injections of MG132, a peptide aldehyde inhibitor of the proteasome (Fig. 7A) (*46*, *47*). We observed that MG132 treatment for 10 days increased protein expression of PKP2, JUP, and DSP in $Pkp2^{c.1755delA/WT}$ mice, whereas DSG and DSC protein expression remained unchanged (Fig. 7, B and C). In addition, α-CAT was also increased, whereas β-CAT and N-CAD showed trends toward up-regulation (Fig. 7, D and E).

Earlier studies used tamoxifen-induced cardiomyocyte-specific deletion of *Pkp2* in adult mice to illustrate that the absence of PKP2 caused increased ryanodine receptor sensitivity toward calcium induction, enhanced sarcoplasmic reticulum calcium load, and an increase in the frequency and amplitude of spontaneous calcium release (*17*–*19*). These findings led us to examine whether desmosomal protein up-regulation achieved through UPS inhibition could correct calcium dysregulation in $Pkp2^{c.1755delA/WT}$ mice. Cardiomyocytes isolated from saline-treated $Pkp2^{c.1755delA/WT}$ mice showed increased calcium amplitude and a reduction in top peak width (10% of total peak duration) at baseline when compared with controls (Fig. 7F). In addition, these cardiomyocytes did not respond to acute isoproterenol exposure. These alterations in calcium dynamics were rescued in cardiomyocytes derived from MG132-treated $Pkp2^{c.1755delA/WT}$ mice, demonstrated

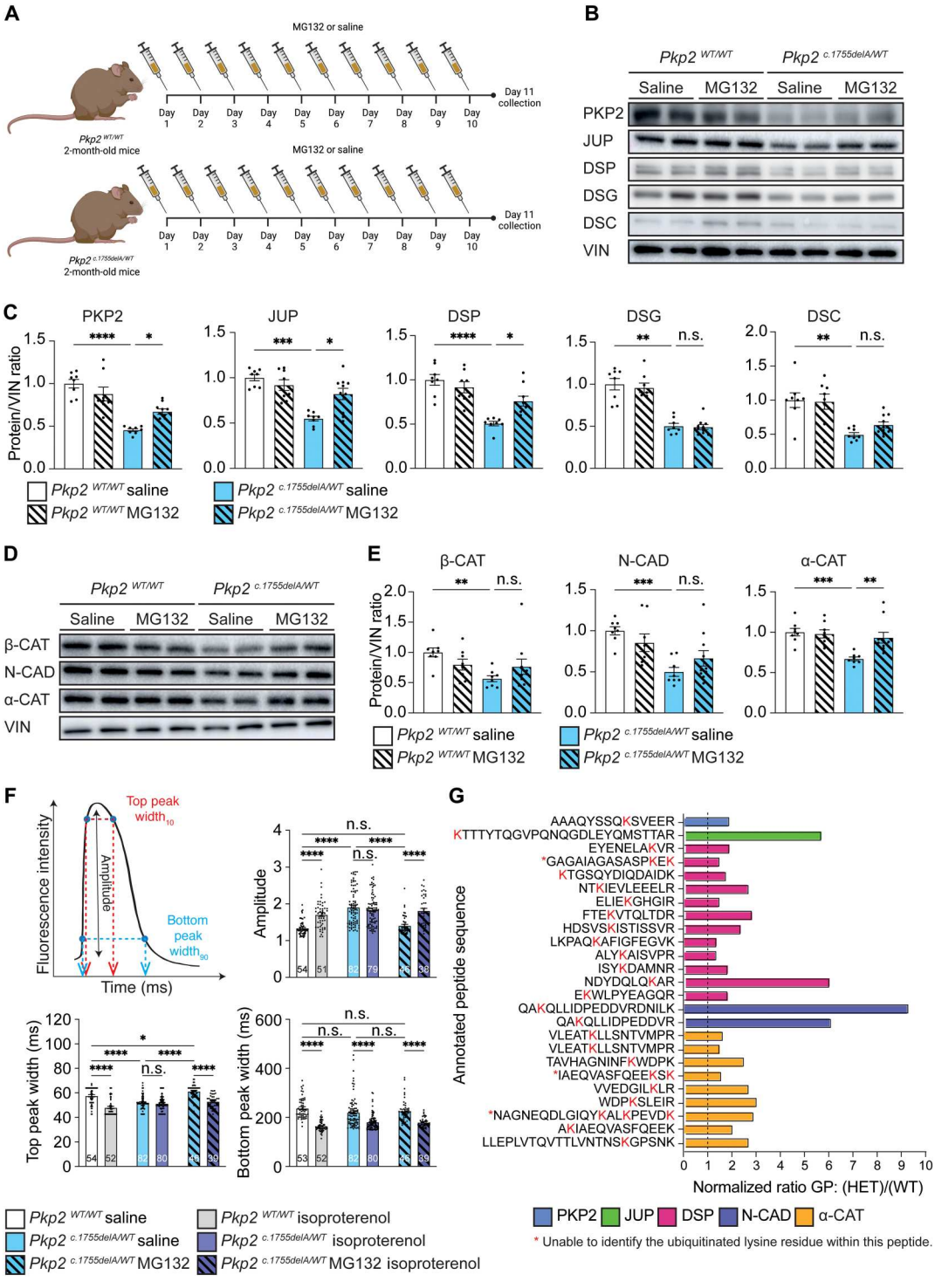

Fig. 7. UPS inhibition in *Pkp2*$^{c.1755delA/WT}$ mice increases desmosomal protein abundance and improves calcium dysregulation. (**A**) Schematic outlining UPS inhibition treatment with MG132 in 8-week-old mice. (**B** to **E**) Representative immunoblots ($n = 2$ per group) and the respective quantification for desmosomal (B and C) and AJ (D and E) proteins on ventricular tissue obtained from mice treated with saline or MG132 ($n = 8$ to 10 mice per group). (**F**) Assessment of calcium transients in cardiomyocytes obtained from Langendorff-perfused mouse hearts treated with saline or MG132 ($n = 3$ mice per group). Isolated cardiomyocytes were treated with either vehicle or isoproterenol. Shown are the calcium transient amplitude, top peak width (10% of total peak duration), and bottom peak width (90% of total peak duration). (**G**) Abundance of desmosomal and AJ protein ubiquitination in ventricular tissue obtained from *Pkp2*$^{WT/WT}$ and *Pkp2*$^{c.1755delA/WT}$ mice using proteomics combined with enrichment for diglycine peptides (ubiquitinated proteins). Lysine (K) residues marked in red were ubiquitinated. Protein expression and electrophysiology data (C, E, and F) were plotted as means ± SEM. (C and E), and significance has been assessed by a Kruskal-Wallis test with Dunn's multiple comparison test; $\alpha = 0.05$. For (F), significance has been assessed by an ordinary two-way ANOVA test with Tukey's multiple comparison test with a single pooled variance (*$P < 0.05$; **$P < 0.01$; ***$P < 0.001$; ****$P < 0.0001$). GP, global proteome abundance; HET, *Pkp2*$^{c.1755delA/WT}$ mice; WT, *Pkp2*$^{WT/WT}$ mice.

by a reduction of the baseline calcium amplitude, an increase in top peak width, and recovery of the acute isoproterenol response (Fig. 7F).

Because of toxicity caused by UPS inhibition (*46*), nonspecific inhibition is not a viable treatment option; instead, a more specific inhibition target will be required (*48*). We aimed to identify the specific protein ubiquitination sites on the target proteins in the presence of this pathological mutation. Ubiquitination of a target protein involves three ligase enzymes, E1 (ubiquitin-activating), E2 (ubiquitin-conjugating). and E3 (substrate-binding) ligases, where substrate specificity is conferred by the E3 ligase (*49*, *50*). Because of the low stoichiometry of ubiquitinated proteins, efforts to decipher the cardiac ubiquitinome through mass spectrometry proteomics have been challenging (*49*). Enrichment for

ubiquitinated proteins through genetically engineered tagged ubiquitin is laborious and suffers from interference from endogenous proteins (*51*, *52*). In this study, we took advantage of highly specific antibodies that recognize the residual diglycine remnant present at substrate ubiquitination lysine sites after trypsin cleavage, allowing us to enrich for ubiquitinated proteins before mass spectrometry analysis (*52*, *53*). By performing ubiquitin proteomics analysis on WT and $Pkp2^{c.1755delA/WT}$ mouse heart samples, we identified a total of 1920 differentially regulated ubiquitinated protein sites when compared with controls. A total of 1722 protein sites (from 534 proteins) demonstrated increased ubiquitination in $Pkp2^{c.1755delA/WT}$ hearts compared with WT hearts. The top 50 most ubiquitinated protein sites in $Pkp2^{c.1755delA/WT}$ hearts are shown in table S4 (the full list can be found at ProteomeXchange Consortium, Proteomics Identification Database, PXD032964). We identified lysine (K) ubiquitination site(s) on desmosomal and AJ proteins that were enriched in $Pkp2^{c.1755delA/WT}$ hearts, including PKP2 (K134), JUP (K57), DSP (K166, K871, K1045, K1166, K1206, K2373, K2535, K2614, K2715, K2738, and K2808), N-CAD (K766), and α-CAT (K12, K16, K45, K163, K577, and K683) (Fig. 7G). Together, these data indicate that the observed protein degradation in $Pkp2^{c.1755delA/WT}$ mice is, at least in part, mediated by the UPS consequent to ubiquitination on target proteins.

DISCUSSION

In the present study, we demonstrate that a single nonsense mutation in *PKP2*, which causes haploinsufficiency of *PKP2*, results in a reduction of other desmosomal and AJ proteins. From patient in vitro and in vivo data, we hypothesize that this molecular phenotype may contribute to the subsequent histological and functional hallmarks observed in ACM. Although the UPS has been shown to be involved in other cardiomyopathies (*54*), we show here that inhibition of the UPS machinery effectively increased protein expression of PKP2, JUP, DSP, and AJ proteins. In addition, this was sufficient to rescue calcium dysregulation in *Pkp2* mutant cardiomyocytes. Ubiquitin proteomics analysis identified specific ubiquitination sites on the target proteins and demonstrated an increased amount of ubiquitination on PKP2 itself and other target proteins in mutant samples. The fact that a single heterozygous mutation in *PKP2* can trigger such a decrease in desmosomal and AJ proteins, resulting in calcium dysregulation, stresses the importance of sufficient quantities of properly functioning PKP2 for cardiac physiology and opens up new avenues for developing therapeutics.

It has been debated whether this widespread decline in desmosomal proteins is specific for patients with ACM, because it was not apparent in patients with other (non)genetic cardiomyopathies or in patients bearing *DSG2* mutations (*21*, *24*). A reduction in desmosomal proteins has only been observed in certain forms of myocarditis (*55*). Here, we demonstrate that reduced PKP2 correlated with reduced protein expression of desmosomal and AJ proteins in patients with ACM. This phenotype was also evident in patients with ACM with other genetic mutations, suggesting a broader effect that could potentially be applicable to other genetic cardiac diseases, which cause PKP2 insufficiency.

The decline in desmosomal protein abundance caused by a *PKP2* mutation is supported by our patient data and recapitulated in our model systems. Furthermore, our data show that the observed protein reduction is posttranslationally regulated, at least partially, through the UPS pathway. This concurs with an earlier neonatal rat cardiomyocyte study showing that the absence of PKP2 resulted in DSP decline, which was rescued through UPS inhibition (*15*). PKP2 is important for both desmosomal protein anchoring and stability; thus, its absence may cause desmosome instability and subsequent degradation of area composita complex proteins (*8*, *56*). Studies conducted in various models, including hiPSC-CMs, zebrafish, and mice, have consistently demonstrated that reduction or loss of desmosomal proteins altered morphology and ID region widening (*26*, *27*, *57*, *58*). In addition to changes in structural integrity, desmosomal proteins interact with other macromolecular structures within the ID, including ion channels, gap junction components, scaffolding, and signaling molecules (*6*, *8*, *11*, *12*). Activation of the Wnt and Yes-associated protein 1 (YAP) pathway causes cardiomyocyte growth, survival, and regeneration, and both are inhibited in ACM pathology (*14*, *59*). Reduction of DSP has been shown to cause JUP nuclear translocation, which competes with β-CAT (a transcriptional coactivator in canonical Wnt signaling) for binding with T cell factor/lymphoid enhancer factor 1 (TCF/LEF1) (transcription factors), thus reducing TCF/LEF1-directed transcription (*14*). PKP2 acts as a scaffold for protein kinase Cα (PKCα) localization with DSP, which is necessary for Merlin inhibition. Activation of Merlin not only prevents YAP transcriptional activity through cytoplasmic retention and degradation but also activates the Hippo pathway, resulting in Wnt signaling inhibition (*13*, *16*).

On the basis of data from our *Pkp2* mutant mice, the decline in desmosomal proteins appears to precede the histological defects, which would be in accordance with patients initially being asymptomatic (*1*–*3*). Furthermore, we show that disorganization of desmosomal and AJ proteins predominantly occurs in regions of extensive fibrotic remodeling in mutant aged mice; this was also shown in explanted human hearts. Age is a heart disease risk factor, originating from escalation of oxidative stress and inflammatory factors (*60*, *61*). In addition, studies have shown that patients with ACM have more severe oxidative stress (*61*, *62*). This implies that local cues and neighboring cell types, combined with external factors such as age, may influence disease severity and penetrance depending on the local stress caused by inherent differences in regional myocardial stress and strain during each cycle of cardiac contraction and relaxation (*63*).

Until now, genetic deletion of *Pkp2* or overexpression of mutated PKP2 in mice has been used to study the relevance of PKP2 in ACM. The deletion mouse models include a whole-body deletion (*Pkp2*-null) or inducible cardiomyocyte-specific deletion [*Pkp2* floxed allele crossed with α-myosin heavy chain–Cre-ER(T2)] (*17*, *19*, *35*, *56*, *64*, *65*). *Pkp2*-null mice were embryonic lethal [embryonic day 10.5 (E10.5) to E11], and inducible deletion at adult stage neglects the impact of PKP2 during development and the effect of PKP2 on other cardiac cell types (*17*, *19*, *35*, *56*, *65*). These models have greatly expanded our understanding of ACM; however, they do not reflect the genetic context observed in patients, because the vast majority of pathogenic mutations are heterozygous point mutations (*1*–*3*). In this study, we generated a heterozygous knockin mouse model of a human pathological *PKP2* variant to better resemble the genetic situation in patients. This mutation caused haploinsufficiency of PKP2 and reduction of other desmosomal proteins, which was accompanied by disorganization of area composita proteins in regions of fibrotic remodeling, resulting in

cardiac dysfunction (*4*). Dysregulation of the AJ proteins was evident in our mouse model, which is intriguing because dysregulation of β-CAT has been shown to drive ACM, and both N-CAD and α-CAT have been linked to ACM (*13*, *40*–*42*, *66*). These molecular changes have not been fully recapitulated in currently available *Pkp2*-related ACM mouse models (*10*, *13*, *20*–*25*). Previous studies demonstrated that homozygous *Pkp2*-null mice suffered from increased instability of JUP, DSP, and DSG; however, the more clinically relevant heterozygous *Pkp2*-null mice had normal expression of desmosomal and N-CAD proteins (*35*, *56*, *67*). At this point, it is unclear whether these differences can be attributed to a dose-responsive phenomenon or whether all nonsense mutations in *Pkp2* would lead to comparable effects. Patients with ACM harboring different *PKP2* mutations also displayed reduced expression of desmosomal and AJ proteins. This suggests that haploinsufficient mutations or the previously reported increased sensitivity of mutant proteins to calcium-dependent calpain proteases could lead to a reduction of PKP2 protein expression, thus driving ACM pathogenesis (*29*, *30*).

In this study, we have shown that UPS inhibition in mutant mice is sufficient to rescue desmosomal protein expression of PKP2, JUP, and DSP. However, nonspecific UPS inhibition would not be a feasible therapeutic strategy, because cellular processes heavily rely on the UPS for removal of misfolded aggregates and toxic proteins to prevent proteotoxicity for the maintenance of proteostasis (*54*). Through ischemic reperfusion studies on mice, rats, and pigs, short-term UPS inhibition has been shown to confer cardioprotection (*68*–*70*). This was demonstrated to be partially due to its anti-inflammatory properties, achieved by prevention of UPS degradation of the inhibitory subunit, inhibitor of κB, which inhibits nuclear factor κB (*68*–*70*). However, cardiotoxicity of long-term UPS inhibitor treatments has been highlighted in many cancer-related clinical studies (*48*). We therefore only use UPS inhibition as a proof of concept to demonstrate the involvement of the UPS in the development of ACM caused by inadequate quantities of PKP2. The identification of the specific PKP2 ubiquitination site in our ubiquitin proteomics strategy may be useful for the development of small molecular inhibitors directed against the PKP2 ubiquitination site or against specific E3 ligases. The peptide sequence surrounding these ubiquitination sites is conserved between mouse and human, suggesting that targeting these sites may have translational potential.

Although the presented in vitro and ex vivo human data provide important insights into ACM pathogenesis, it remains difficult to extrapolate these findings to the clinic. On one hand, the hiPSC-CMs are known for their fetal-like state, whereas the explanted human ACM hearts resemble end-stage disease characteristics. The use of more advanced maturation protocols and inclusion of clinical parameters in future studies may contribute to a better understanding and translation of our findings. In addition, although our mouse model displayed many ACM hallmarks, adipose remodeling was not evident for the duration of our study. Therefore, it is possible that introducing additional stress to this model would induce a more pronounced ACM phenotype that is currently not evident at baseline conditions.

In conclusion, our results indicate that mutations found in patients with ACM, particularly *PKP2 c.2013delC*, lead to a decline in desmosomal and AJ proteins and cardiac function that may be mediated by the UPS. Our data demonstrate the importance of using relevant disease models to identify disease-driving mechanisms for the development of new therapeutic strategies.

MATERIALS AND METHODS

Study design

The main objective of this project was to identify disease-driving mechanisms underlying ACM by combining in vitro and in vivo models. Patients with ACM and control heart samples were obtained from the University Medical Center Utrecht Biobank. Biobank material collection was approved by the scientific advisory board of the Biobank of the University Medical Center Utrecht, Netherlands (protocol nos. 12/387 and 15–252). Written informed consent was obtained from all patients. Details of the sample collection and immunoblot and immunohistochemistry procedures are listed in the Supplementary Materials.

$Pkp2^{c.1755delA/WT}$ mice were generated by modifying 129/Ola-derived IB10 cells (provided by the Netherlands Cancer Institute, Amsterdam) with CRISPR-Cas9. Modified cells were injected into blastocysts derived from B6 mice and subsequently injected into pseudopregnant B6 mice. Chimeric offspring were crossbred with C57BL/6 mice. Ventricular cardiac tissue was obtained from 2-, 4-, and 12-month-old $Pkp2^{c.1755delA/WT}$ and $Pkp2^{WT/WT}$ mice. Detailed procedures regarding generation of the $Pkp2^{c.1755delA/WT}$ mouse line, sample collection, molecular assays, and MG132 treatment strategy are listed in the Supplementary Materials. The number of mice was chosen on the basis of power analysis to provide adequate statistical power. Only male mice were used, because ACM has a male predominance (*71*). Animal experiments were randomized and blinded for genotype and treatment and were performed in accordance with institutional guidelines and regulations of the Animal Welfare Committee of the Royal Netherlands Academy of Arts and Sciences.

The $PKP2^{c.2013delC/WT}$ hiPSC line has been previously described in "Studying arrhythmogenic right ventricular dysplasia with patient-specific iPSCs" (*32*). All molecular work has been performed on 1-month-old hiPSC-CMs. All in vitro experiments were performed on at least three independent cardiomyocyte differentiations. Sample collection and experimental procedures are described in detail in the Supplementary Materials.

Statistical analysis

Numeric values are reported as means ± SEM. Outliers were identified and removed using the robust regression and outlier removal (ROUT) method (Q = 5%). Correlation and significance between proteins have been assessed by nonparametric Spearman correlation (two-tailed, 95% confidence interval). A chi-square test was used to assess significance for the functional data obtained for MTs. For comparison between two groups, significance has been assessed by a two-tailed unpaired Student's t test or two-tailed Mann-Whitney test when data were not normally distributed (Kolmogorov-Smirnov test). A two-way repeated-measures analysis of variance (ANOVA) followed by Holm-Sidak test for post hoc analysis was applied for comparison of I_{Na} densities in hiPSC-CMs. For comparison between three and more groups, a one-way ANOVA Kruskal-Wallis test with Dunn's multiple comparison test; α = 0.05 was performed. Statistical tests and graphs were done with GraphPad Prism 9. NDP.view2 software (Hamamatsu) was used for analyzing immunostainings on human tissue. ImageJ2 version

2.3.0/1.53f was used for analysis and quantification of immunoblots and immunostainings performed on mouse and hiPSC-CM samples. Detailed description of the statistics for each experiment and for the mass spectrometry experiments are reported in the figure legends and Supplementary Materials, respectively.

Supplementary Materials

This PDF file includes:
Materials and Methods
Figs. S1 to S10
Tables S1 to S11
References (*72*–*82*)

Other Supplementary Material for this manuscript includes the following:
Data file S1
MDAR Reproducibility Checklist

View/request a protocol for this paper from *Bio-protocol*.

REFERENCES AND NOTES

1. K. Pilichou, G. Thiene, B. Bauce, I. Rigato, E. Lazzarini, F. Migliore, M. Perazzolo Marra, S. Rizzo, A. Zorzi, L. Daliento, D. Corrado, C. Basso, Arrhythmogenic cardiomyopathy. *Orphanet J. Rare Dis.* **11**, 33 (2016).
2. F. I. Marcus, W. J. McKenna, D. Sherrill, C. Basso, B. Bauce, D. A. Bluemke, H. Calkins, D. Corrado, M. G. P. J. Cox, J. P. Daubert, G. Fontaine, K. Gear, R. Hauer, A. Nava, M. H. Picard, N. Protonotarios, J. E. Saffitz, D. M. Y. Sanborn, J. S. Steinberg, H. Tandri, G. Thiene, J. A. Towbin, A. Tsatsopoulou, T. Wichter, W. Zareba, Diagnosis of arrhythmogenic right ventricular cardiomyopathy/dysplasia. *Eur. Heart J.* **31**, 806–814 (2010).
3. K. M. Austin, M. A. Trembley, S. F. Chandler, S. P. Sanders, J. E. Saffitz, D. J. Abrams, W. T. Pu, Molecular mechanisms of arrhythmogenic cardiomyopathy. *Nat. Rev. Cardiol.* **16**, 519–537 (2019).
4. D. Corrado, M. S. Link, H. Calkins, Arrhythmogenic right ventricular cardiomyopathy. *N. Engl. J. Med.* **376**, 61–72 (2017).
5. A. Lorenzon, M. Calore, G. Poloni, L. J. De Windt, P. Braghetta, A. Rampazzo, Wnt/β-catenin pathway in arrhythmogenic cardiomyopathy. *Oncotarget* **8**, 60640–60655 (2017).
6. D. M. Patel, K. J. Green, Desmosomes in the heart: A review of clinical and mechanistic analyses. *Cell Commun. Adhes.* **21**, 109–128 (2014).
7. S. Sepehrkhouy, J. M. I. H. Gho, R. van Es, M. Harakalova, N. de Jonge, D. Dooijes, J. J. van der Smagt, M. P. Buijsrogge, R. N. W. Hauer, R. Goldschmeding, R. A. de Weger, F. W. Asselbergs, A. Vink, Distinct fibrosis pattern in desmosomal and phospholamban mutation carriers in hereditary cardiomyopathies. *Heart Rhythm* **14**, 1024–1032 (2017).
8. S. H. Vermij, H. Abriel, T. A. B. van Veen, Refining the molecular organization of the cardiac intercalated disc. *Cardiovasc. Res.* **113**, 259–275 (2017).
9. W. W. Franke, C. M. Borrmann, C. Grund, S. Pieperhoff, The area composita of adhering junctions connecting heart muscle cells of vertebrates. I. Molecular definition in intercalated disks of cardiomyocytes by immunoelectron microscopy of desmosomal proteins. *Eur. J. Cell Biol.* **85**, 69–82 (2006).
10. S. R. Kaplan, J. J. Gard, N. Protonotarios, A. Tsatsopoulou, C. Spiliopoulou, A. Anastasakis, C. P. Squarcioni, W. J. McKenna, G. Thiene, C. Basso, N. Brousse, G. Fontaine, J. E. Saffitz, Remodeling of myocyte gap junctions in arrhythmogenic right ventricular cardiomyopathy due to a deletion in plakoglobin (Naxos disease). *Heart Rhythm* **1**, 3–11 (2004).
11. A. Vite, G. L. Radice, N-cadherin/catenin complex as a master regulator of intercalated disc function. *Cell Commun. Adhes.* **21**, 169–179 (2014).
12. P. Y. Sato, W. Coombs, X. Lin, O. Nekrasova, K. Green, L. L. Isom, S. Taffet, M. Delmar, Interactions between ankyrin-G, plakophilin-2 and connexin43 at the cardiac intercalated disc. *Circ. Res.* **109**, 193–201 (2011).
13. S. N. Chen, P. Gurha, R. Lombardi, A. Ruggiero, J. T. Willerson, A. J. Marian, The hippo pathway is activated and is a causal mechanism for adipogenesis in arrhythmogenic cardiomyopathy. *Circ. Res.* **114**, 454–468 (2014).
14. E. Garcia-gras, R. Lombardi, M. J. Giocondo, J. T. Willerson, M. D. Schneider, D. S. Khoury, A. J. Marian, Suppression of canonical Wnt/β-catenin signaling by nuclear plakoglobin recapitulates phenotype of arrhythmogenic right ventricular cardiomyopathy. *J. Clin. Investig.* **116**, 2012–2021 (2006).
15. A. D. Dubash, C. Y. Kam, B. A. Aguado, D. M. Patel, M. Delmar, L. D. Shea, K. J. Green, Plakophilin-2 loss promotes TGF-β1/p38 MAPK-dependent fibrotic gene expression in cardiomyocytes. *J. Cell Biol.* **212**, 425–438 (2016).
16. A. E. Bass-Zubek, R. P. Hobbs, E. V. Amargo, N. J. Garcia, S. N. Hsieh, X. Chen, J. K. Wahl, M. F. Denning, K. J. Green, Plakophilin 2: A critical scaffold for PKCα that regulates intercellular junction assembly. *J. Cell Biol.* **181**, 605–613 (2008).
17. J.-C. Kim, M. Pérez-Hernández, J. Alvarado Francisco, R. Maurya Svetlana, J. Montnach, Y. Yin, M. Zhang, X. Lin, C. Vasquez, A. Heguy, F.-X. Liang, S.-H. Woo, E. Morley Gregory, E. Rothenberg, A. Lundby, H. Valdivia Hector, M. Cerrone, M. Delmar, Disruption of $Ca2_i^+$ homeostasis and connexin 43 hemichannel function in the right ventricle precedes overt arrhythmogenic cardiomyopathy in PKP2-deficient mice. *Circulation* **140**, 1015–1030 (2019).
18. C. J. M. v. Opbergen, N. Bagwan, S. R. Maurya, J.-C. Kim, A. N. Smith, D. J. Blackwell, J. N. Johnston, B. C. Knollmann, Marina Cerrone, A. Lundby, M. Delmar, Exercise causes arrhythmogenic remodeling of intracellular calcium dynamics in plakophilin-2–deficient hearts. *Circulation* **145**, 1480–1496 (2022).
19. M. Cerrone, J. Montnach, X. Lin, Y.-T. Zhao, M. Zhang, E. Agullo-Pascual, A. Leo-Macias, F. J. Alvarado, I. Dolgalev, T. V. Karathanos, K. Malkani, C. J. M. Van Opbergen, J. J. A. van Bavel, H.-Q. Yang, C. Vasquez, D. Tester, S. Fowler, F. Liang, E. Rothenberg, A. Heguy, G. E. Morley, W. A. Coetzee, N. A. Trayanova, M. J. Ackerman, T. A. B. van Veen, H. H. Valdivia, M. Delmar, Plakophilin-2 is required for transcription of genes that control calcium cycling and cardiac rhythm. *Nat. Commun.* **8**, 106 (2017).
20. T. B. Rasmussen, P. H. Nissen, J. Palmfeldt, K. Gehmlich, S. Dalager, U. B. Jensen, W. Y. Kim, L. Heickendorff, H. Mlgaard, H. K. Jensen, U. T. Baandrup, P. Bross, J. Mogensen, Truncating plakophilin-2 mutations in arrhythmogenic cardiomyopathy are associated with protein haploinsufficiency in both myocardium and epidermis. *Circ. Cardiovasc. Genet.* **7**, 230–240 (2014).
21. A. Asimaki, H. Tandri, H. Huang, M. K. Halushka, S. Gautam, C. Basso, G. Thiene, A. Tsatsopoulou, N. Protonotarios, W. J. McKenna, H. Calkins, J. E. Saffitz, A new diagnostic test for arrhythmogenic right ventricular cardiomyopathy. *N. Engl. J. Med.* **360**, 1075–1084 (2009).
22. S. R. Kaplan, J. J. Gard, L. Carvajal-Huerta, J. C. Ruiz-Cabezas, G. Thiene, J. E. Saffitz, Structural and molecular pathology of the heart in Carvajal syndrome. *Cardiovasc. Pathol.* **13**, 26–32 (2004).
23. H. Tandri, A. Asimaki, D. Dalal, J. E. Saffitz, M. K. Halushka, H. Calkins, Gap junction remodeling in a case of arrhythmogenic right ventricular dysplasia due to plakophilin-2 mutation. *J. Cardiovasc. Electrophysiol.* **19**, 1212–1214 (2008).
24. A. Vite, E. Gandjbakhch, C. Prost, V. Fressart, P. Fouret, N. Neyroud, F. Gary, E. Donal, S. Varnous, G. Fontaine, P. Fornes, F. Hidden-Lucet, M. Komjada, P. Charron, E. Villard, Desmosomal cadherins are decreased in explanted arrhythmogenic right ventricular dysplasia/ cardiomyopathy patient hearts. *PLOS ONE* **8**, e75082 (2013).
25. M. Noorman, S. Hakim, E. Kessler, J. A. Groeneweg, M. G. P. J. Cox, A. Asimaki, H. V. M. van Rijen, L. van Stuijvenberg, H. Chkourko, M. A. G. van Der Heyden, M. A. Vos, N. De Jonge, J. J. van Der Smagt, D. Dooijes, A. Vink, R. A. de Weger, A. Varro, J. M. T. De Bakker, J. E. Saffitz, T. J. Hund, P. J. Mohler, M. Delmar, R. N. W. Hauer, T. A. B. van Veen, Remodeling of the cardiac sodium channel, connexin43, and plakoglobin at the intercalated disk in patients with arrhythmogenic cardiomyopathy. *Heart Rhythm* **10**, 412–419 (2013).
26. O. Caspi, I. Huber, A. Gepstein, G. Arbel, L. Maizels, M. Boulos, L. Gepstein, Modeling of arrhythmogenic right ventricular cardiomyopathy with human induced pluripotent stem cells. *Circ. Cardiovasc. Genet.* **6**, 557–568 (2013).
27. S. Kant, B. Holthöfer, M. Magin Thomas, A. Krusche Claudia, E. Leube Rudolf, Desmoglein 2–dependent arrhythmogenic cardiomyopathy is caused by a loss of adhesive function. *Circ. Cardiovasc. Genet.* **8**, 553–563 (2015).
28. C. Wang, X. Wang, The interplay between autophagy and the ubiquitin–proteasome system in cardiac proteotoxicity. *Biochim. Biophys. Acta* **1852**, 188–194 (2015).
29. F. Kirchner, A. Schuetz, L.-H. Boldt, K. Martens, G. Dittmar, W. Haverkamp, L. Thierfelder, U. Heinemann, B. Gerull, Molecular insights into arrhythmogenic right ventricular cardiomyopathy caused by plakophilin-2 missense mutations. *Circ. Cardiovasc. Genet.* **5**, 400–411 (2012).
30. R. Ng, H. Manring, N. Papoutsidakis, T. Albertelli, N. Tsai, C. J. See, X. Li, J. Park, T. L. Stevens, P. J. Bobbili, M. Riaz, Y. Ren, C. E. Stoddard, P. M. L. Janssen, T. J. Bunch, S. P. Hall, Y.-C. Lo, D. L. Jacoby, Y. Qyang, N. Wright, M. A. Ackermann, S. G. Campbell, Patient mutations linked to arrhythmogenic cardiomyopathy enhance calpain-mediated desmoplakin degradation. *JCI Insight* **4**, e128643 (2019).
31. Y. Liang, R. C. Lyon, J. Pellman, W. H. Bradford, S. Lange, J. Bogomolovas, N. D. Dalton, Y. Gu, M. Bobar, M.-H. Lee, T. Iwakuma, V. Nigam, A. Asimaki, M. Scheinman, K. L. Peterson, F. Sheikh, Desmosomal COP9 regulates proteome degradation in arrhythmogenic right ventricular dysplasia/cardiomyopathy. *J. Clin. Invest.* **131**, e137689 (2021).
32. C. Kim, J. Wong, J. Wen, S. Wang, C. Wang, S. Spiering, N. G. Kan, S. Forcales, P. L. Puri, T. C. Leone, J. E. Marine, H. Calkins, D. P. Kelly, D. P. Judge, H.-S. V. Chen, Studying

arrhythmogenic right ventricular dysplasia with patient-specific iPSCs. *Nature* **494**, 105–110 (2013).
33. A. Kohela, S. J. van Kampen, T. Moens, M. Wehrens, B. Molenaar, C. J. Boogerd, J. Monshouwer-Kloots, I. Perini, M. J. Goumans, A. M. Smits, J. P. van Tintelen, E. van Rooij, Epicardial differentiation drives fibro-fatty remodeling in arrhythmogenic cardiomyopathy. *Sci. Transl. Med.* **13**, eabf2750 (2021).
34. P. Y. Sato, H. Musa, W. Coombs, G. Guerrero-Serna, G. A. Patiño, S. M. Taffet, L. L. Isom, M. Delmar, Loss of plakophilin-2 expression leads to decreased sodium current and slower conduction velocity in cultured cardiac myocytes. *Circ. Res.* **105**, 523–526 (2009).
35. M. Cerrone, M. Noorman, X. Lin, H. Chkourko, F.-X. Liang, R. van der Nagel, T. Hund, W. Birchmeier, P. Mohler, T. A. van Veen, H. V. van Rijen, M. Delmar, Sodium current deficit and arrhythmogenesis in a murine model of plakophilin-2 haploinsufficiency. *Cardiovasc. Res.* **95**, 460–468 (2012).
36. E. Giacomelli, V. Meraviglia, G. Campostrini, A. Cochrane, X. Cao, R. W. J. van Helden, A. K. Garcia, M. Mircea, S. Kostidis, R. P. Davis, B. J. van Meer, C. R. Jost, A. J. Koster, H. Mei, D. G. Míguez, A. A. Mulder, M. Ledesma-Terrón, G. Pompilio, L. Sala, D. C. F. Salvatori, R. C. Slieker, E. Sommariva, A. A. F. de Vries, M. Giera, S. Semrau, L. G. J. Tertoolen, V. V. Orlova, M. Bellin, C. L. Mummery, Human-iPSC-derived cardiac stromal cells enhance maturation in 3D cardiac microtissues and reveal non-cardiomyocyte contributions to heart disease. *Cell Stem Cell* **26**, 862–879.e11 (2020).
37. G. Campostrini, V. Meraviglia, E. Giacomelli, R. W. J. van Helden, L. Yiangou, R. P. Davis, M. Bellin, V. V. Orlova, C. L. Mummery, Generation, functional analysis and applications of isogenic three-dimensional self-aggregating cardiac microtissues from human pluripotent stem cells. *Nat. Protoc.* **16**, 2213–2256 (2021).
38. L. Zhang, L. Liu, P. Kowey, G. Fontaine, The electrocardiographic manifestations of arrhythmogenic right ventricular dysplasia. *Curr. Cardiol. Rev.* **10**, 237–245 (2014).
39. W. Wang, C. A. James, H. Calkins, Diagnostic and therapeutic strategies for arrhythmogenic right ventricular dysplasia/cardiomyopathy patient. *Europace* **21**, 9–21 (2019).
40. B. M. Mayosi, M. Fish, G. Shaboodien, E. Mastantuono, S. Kraus, T. Wieland, M.-C. Kotta, A. Chin, N. Laing, N. B. A. Ntusi, M. Chong, C. Horsfall, S. N. Pimstone, D. Gentilini, G. Parati, T.-M. Strom, T. Meitinger, G. Pare, P. J. Schwartz, L. Crotti, Identification of cadherin 2 (*CDH2*) mutations in arrhythmogenic right ventricular cardiomyopathy. *Circ. Cardiovasc. Genet.* **10**, e001605 (2017).
41. F. Sheikh, Y. Chen, X. Liang, A. Hirschy, A. E. Stenbit, Y. Gu, N. D. Dalton, T. Yajima, Y. Lu, K. U. Knowlton, K. L. Peterson, J.-C. Perriard, J. Chen, α-E-Catenin inactivation disrupts the cardiomyocyte adherens junction, resulting in cardiomyopathy and susceptibility to wall rupture. *Circulation* **114**, 1046–1055 (2006).
42. S. E. Chiarella, E. E. Rabin, L. A. Ostilla, A. S. Flozak, C. J. Gottardi, αT-catenin: A developmentally dispensable, disease-linked member of the α-catenin family. *Tissue Barriers* **6**, e1463896 (2018).
43. I. San Román, M. Navarro, F. Martínez, L. Albert, L. Polo, J. Guardiola, E. García-Molina, C. Muñoz-Esparza, J. M. López-Ayala, M. Sabater-Molina, J. R. Gimeno, Unclassifiable arrhythmic cardiomyopathy associated with Emery-Dreifuss caused by a mutation in FHL1. *Clin. Genet.* **90**, 171–176 (2016).
44. J. M. Lopez-Ayala, M. Ortiz-Genga, I. Gomez-Milanes, D. Lopez-Cuenca, F. Ruiz-Espejo, J. J. Sanchez-Munoz, M. J. Oliva-Sandoval, L. Monserrat, J. R. Gimeno, A mutation in the Z-line Cypher/ZASP protein is associated with arrhythmogenic right ventricular cardiomyopathy. *Clin. Genet.* **88**, 172–176 (2015).
45. K. Zientara-Rytter, S. Subramani, The roles of ubiquitin-binding protein shuttles in the degradative fate of ubiquitinated proteins in the ubiquitin-proteasome system and autophagy. *Cell* **8**, 40 (2019).
46. A. F. Kisselev, A. L. Goldberg, Proteasome inhibitors: From research tools to drug candidates. *Chem. Biol.* **8**, 739–758 (2001).
47. X.-M. Zhang, Y.-C. Li, P. Chen, S. Ye, S.-H. Xie, W.-J. Xia, J.-H. Yang, MG-132 attenuates cardiac deterioration of viral myocarditis via AMPK pathway. *Biomed. Pharmacother.* **126**, 110091 (2020).
48. A. Das, S. Dasgupta, Y. Gong, U. A. Shah, M. G. Fradley, R. K. Cheng, B. Roy, A. Guha, Cardiotoxicity as an adverse effect of immunomodulatory drugs and proteasome inhibitors in multiple myeloma: A network meta-analysis of randomized clinical trials. *Hematol. Oncol.* **40**, 233–242 (2022).
49. P.-C. Chen, C. H. Na, J. Peng, Quantitative proteomics to decipher ubiquitin signaling. *Amino Acids* **43**, 1049–1060 (2012).
50. C. M. Pickart, Back to the future with ubiquitin. *Cell* **116**, 181–190 (2004).
51. H. B. Jeon, E. S. Choi, J. H. Yoon, J. H. Hwang, J. W. Chang, E. K. Lee, H. W. Choi, Z.-Y. Park, Y. J. Yoo, A proteomics approach to identify the ubiquitinated proteins in mouse heart. *Biochem. Biophys. Res. Commun.* **357**, 731–736 (2007).
52. N. D. Udeshi, P. Mertins, T. Svinkina, S. A. Carr, Large-scale identification of ubiquitination sites by mass spectrometry. *Nat. Protoc.* **8**, 1950–1960 (2013).
53. L. van der Wal, K. Bezstarosti, K. A. Sap, D. H. W. Dekkers, E. Rijkers, E. Mientjes, Y. Elgersma, J. A. A. Demmers, Improvement of ubiquitylation site detection by orbitrap mass spectrometry. *J. Proteomics* **172**, 49–56 (2018).
54. J. E. Gilda, A. V. Gomes, Proteasome dysfunction in cardiomyopathies. *J. Physiol.* **595**, 4051–4071 (2017).
55. A. Asimaki, H. Tandri, E. R. Duffy, J. R. Winterfield, S. Mackey-Bojack, M. M. Picken, L. T. Cooper, D. J. Wilber, F. I. Marcus, C. Basso, G. Thiene, A. Tsatsopoulou, N. Protonotarios, W. G. Stevenson, W. J. McKenna, S. Gautam, D. G. Remick, H. Calkins, J. E. Saffitz, Altered desmosomal proteins in granulomatous myocarditis and potential pathogenic links to arrhythmogenic right ventricular cardiomyopathy. *Circ. Arrhythm. Electrophysiol.* **4**, 743–752 (2011).
56. K. S. Grossmann, C. Grund, J. Huelsken, M. Behrend, B. Erdmann, W. W. Franke, W. Birchmeier, Requirement of plakophilin 2 for heart morphogenesis and cardiac junction formation. *J. Cell Biol.* **167**, 149–160 (2004).
57. A. Heuser, E. R. Plovie, P. T. Ellinor, K. S. Grossmann, J. T. Shin, T. Wichter, C. T. Basson, B. B. Lerman, S. Sasse-Klaassen, L. Thierfelder, C. A. MacRae, B. Gerull, Mutant desmocollin-2 causes arrhythmogenic right ventricular cardiomyopathy. *Am. J. Hum. Genet.* **79**, 1081–1088 (2006).
58. R. C. Lyon, V. Mezzano, A. T. Wright, E. Pfeiffer, J. Chuang, K. Banares, A. Castaneda, K. Ouyang, L. Cui, R. Contu, Y. Gu, S. M. Evans, J. H. Omens, K. L. Peterson, A. D. McCulloch, F. Sheikh, Connexin defects underlie arrhythmogenic right ventricular cardiomyopathy in a novel mouse model. *Hum. Mol. Genet.* **23**, 1134–1150 (2013).
59. Y. Hu, W. T. Pu, Hippo activation in arrhythmogenic cardiomyopathy. *Circ. Res.* **114**, 402–405 (2014).
60. C. A. Meschiari, O. K. Ero, H. Pan, T. Finkel, M. L. Lindsey, The impact of aging on cardiac extracellular matrix. *Geroscience* **39**, 7–18 (2017).
61. J. L. Rodgers, J. Jones, S. I. Bolleddu, S. Vanthenapalli, L. E. Rodgers, K. Shah, K. Karia, S. K. Panguluri, Cardiovascular risks associated with gender and aging. *J. Cardiovasc. Dev. Dis.* **6**, 19 (2019).
62. E. Sommariva, I. Stadiotti, M. Casella, V. Catto, A. D. Russo, C. Carbucicchio, L. Arnaboldi, S. De Metrio, G. Milano, A. Scopece, M. Casaburo, A. Andreini, S. Mushtaq, E. Conte, M. Chiesa, W. Birchmeier, E. Cogliati, A. Paolin, E. König, V. Meraviglia, M. De Musso, C. Volani, G. Cattelan, W. Rauhe, L. Turnu, B. Porro, M. Pedrazzini, M. Camera, A. Corsini, C. Tondo, A. Rossini, G. Pompilio, Oxidized LDL-dependent pathway as new pathogenic trigger in arrhythmogenic cardiomyopathy. *EMBO Mol. Med.* **19**, e14365 (2021).
63. O. A. Smiseth, H. Torp, A. Opdahl, K. H. Haugaa, S. Urheim, Myocardial strain imaging: How useful is it in clinical decision making? *Eur. Heart J.* **37**, 1196–1207 (2016).
64. J. Moncayo-Arlandi, E. Guasch, M. S. d. la Garza, M. Casado, N. A. Garcia, L. Mont, M. Sitges, R. Knöll, B. Buyandelger, O. Campuzano, A. Diez-Juan, R. Brugada, Molecular disturbance underlies to arrhythmogenic cardiomyopathy induced by transgene content, age and exercise in a truncated PKP2 mouse model. *Hum. Mol. Genet.* **25**, 3676–3688 (2016).
65. F. M. Cruz, D. Sanz-Rosa, M. Roche-Molina, J. García-Prieto, J. M. García-Ruiz, G. Pizarro, L. J. Jiménez-Borreguero, M. Torres, A. Bernad, J. Ruíz-Cabello, V. Fuster, B. Ibáñez, J. A. Bernal, Exercise triggers ARVC phenotype in mice expressing a disease-causing mutated version of human plakophilin-2. *J. Am. Coll. Cardiol.* **65**, 1438–1450 (2015).
66. J. van Hengel, M. Calore, B. Bauce, E. Dazzo, E. Mazzotti, M. De Bortoli, A. Lorenzon, I. E. Li Mura, G. Beffagna, I. Rigato, M. Vleeschouwers, K. Tyberghein, P. Hulpiau, E. van Hamme, T. Zaglia, D. Corrado, C. Basso, G. Thiene, L. Daliento, A. Nava, F. van Roy, A. Rampazzo, Mutations in the area composita protein αT-catenin are associated with arrhythmogenic right ventricular cardiomyopathy. *Eur. Heart J.* **34**, 201–210 (2013).
67. C. J. M. van Opbergen, M. Noorman, A. Pfenniger, J. S. Copier, S. H. Vermij, Z. Li, R. van der Nagel, M. Zhang, J. M. T. de Bakker, A. M. Glass, P. J. Mohler, S. M. Taffet, M. A. Vos, H. V. M. van Rijen, M. Delmar, T. A. B. van Veen, Plakophilin-2 haploinsuffciency causes calcium handling deficits and modulates the cardiac response towards stress. *Int. J. Mol. Sci.* **20**, 4076 (2019).
68. W. E. Stansfield, N. C. Moss, M. S. Willis, R. Tang, C. H. Selzman, Proteasome inhibition attenuates infarct size and preserves cardiac function in a murine model of myocardial ischemia-reperfusion injury. *Ann. Thorac. Surg.* **84**, 120–125 (2007).
69. B. Adams, R. F. Mapanga, M. F. Essop, Partial inhibition of the ubiquitin-proteasome system ameliorates cardiac dysfunction following ischemia-reperfusion in the presence of high glucose. *Cardiovasc. Diabetol.* **14**, 94 (2015).
70. J. Pye, F. Ardeshirpour, A. McCain, D. A. Bellinger, E. Merricks, J. Adams, P. J. Elliott, C. Pien, T. H. Fischer, A. S. Baldwin, T. C. Nichols, Proteasome inhibition ablates activation of NF-κB in myocardial reperfusion and reduces reperfusion injury. *Am. J. Physiol. Heart. Circ. Physiol.* **284**, H919-26 (2003).
71. D. Akdis, C. Brunckhorst, F. Duru, A. M. Saguner, Arrhythmogenic cardiomyopathy: Electrical and structural phenotypes. *Arrhythm. Electrophysiol. Rev.* **5**, 90–101 (2016).
72. W. E. Louch, K. A. Sheehan, B. M. Wolska, Methods in cardiomyocyte isolation, culture, and gene transfer. *J. Mol. Cell. Cardiol.* **51**, 288–298 (2011).

73. M. I. Love, W. Huber, S. Anders, Moderated estimation of fold change and dispersion for RNA-seq data with DESeq2. *Genome Biol.* **15**, 550 (2014).
74. P. Whittaker, R. A. Kloner, D. R. Boughner, J. G. Pickering, Quantitative assessment of myocardial collagen with picrosirius red staining and circularly polarized light. *Basic Res. Cardiol.* **89**, 397–410 (1994).
75. B. Vogel, H. Siebert, U. Hofmann, S. Frantz, Determination of collagen content within picrosirius red stained paraffin-embedded tissue sections using fluorescence microscopy. *MethodsX* **2**, 124–134 (2015).
76. J. A. Vizcaíno, R. G. Côté, A. Csordas, J. A. Dianes, A. Fabregat, J. M. Foster, J. Griss, E. Alpi, M. Birim, J. Contell, G. O'Kelly, A. Schoenegger, D. Ovelleiro, Y. Pérez-Riverol, F. Reisinger, D. Ríos, R. Wang, H. Hermjakob, The PRoteomics IDEntifications (PRIDE) database and associated tools: Status in 2013. *Nucleic Acids Res.* **41**, D1063–D1069 (2013).
77. Y. Perez-Riverol, A. Csordas, J. Bai, M. Bernal-Llinares, S. Hewapathirana, D. J. Kundu, A. Inuganti, J. Griss, G. Mayer, M. Eisenacher, E. Pérez, J. Uszkoreit, J. Pfeuffer, T. Sachsenberg, S. Yilmaz, S. Tiwary, J. Cox, E. Audain, M. Walzer, A. F. Jarnuczak, T. Ternent, A. Brazma, J. A. Vizcaíno, The PRIDE database and related tools and resources in 2019: Improving support for quantification data. *Nucleic Acids Res.* **47**, D442–D450 (2019).
78. J. Cox, I. Matic, M. Hilger, N. Nagaraj, M. Selbach, J. V. Olsen, M. Mann, A practical guide to the MaxQuant computational platform for SILAC-based quantitative proteomics. *Nat. Protoc.* **4**, 698–705 (2009).
79. A. C. F. Bolhaqueiro, B. Ponsioen, B. Bakker, S. J. Klaasen, E. Kucukkose, R. H. van Jaarsveld, J. Vivié, I. Verlaan-Klink, N. Hami, D. C. J. Spierings, N. Sasaki, D. Dutta, S. F. Boj, R. G. J. Vries, P. M. Lansdorp, M. van de Wetering, A. van Oudenaarden, H. Clevers, O. Kranenburg, F. Foijer, H. J. G. Snippert, G. J. P. L. Kops, Ongoing chromosomal instability and karyotype evolution in human colorectal cancer organoids. *Nat. Genet.* **51**, 824–834 (2019).
80. P. H. Barry, J. W. Lynch, Liquid junction potentials and small cell effects in patch-clamp analysis. *J. Membr. Biol.* **121**, 101–117 (1991).
81. V. Meraviglia, C. H. Arendzen, M. Tok, C. Freund, A. S. Maione, E. Sommariva, M. Bellin, Generation of human induced pluripotent stem cell line LUMCi027-A and its isogenic gene-corrected line from a patient affected by arrhythmogenic cardiomyopathy and carrying the c.2013delC PKP2 mutation. *Stem Cell Res.* **46**, 101835 (2020).
82. M. Zhang, C. D'Aniello, A. O. Verkerk, E. Wrobel, S. Frank, D. Ward-van Oostwaard, I. Piccini, C. Freund, J. Rao, G. Seebohm, D. E. Atsma, E. Schulze-Bahr, C. L. Mummery, B. Greber, M. Bellin, Recessive cardiac phenotypes in induced pluripotent stem cell models of Jervell and Lange-Nielsen syndrome: Disease mechanisms and pharmacological rescue. *Proc. Natl. Acad. Sci. U.S.A.* **111**, E5383–E5392 (2014).

Acknowledgments: We thank F. A. Moqadam and A. R. Leitoguinho for assisting in the design and selection of the gRNAs. **Funding:** This work was supported by the Dutch CardioVascular Alliance with support of the Dutch Heart Foundation, DCVA2017-18 ARENA-PRIME (E.v.R.); Dutch CardioVascular Alliance with support of the Dutch Heart Foundation, DCVA2015-12 eDETECT (T.A.B.v.V. and C.A.R); Dutch CardioVascular Alliance with support of the Dutch Heart Foundation, DCVA2018-30 PREDICT2 (T.A.B.v.V. and C.A.R.); Fondation Leducq Transatlantic Network of Excellence, 17CVD02 (C.A.R.); Vici grant from the Dutch Research Council (NWO), project 09150181910020 (E.v.R.); Gravitation Program "Materials-Driven Regeneration" funded by the Netherlands Organization for Scientific Research, 024.003.013 (C.L.M.); Netherlands Organisation for Health Research and Development (ZonMW), MKMD project 114022504 (C.L.M.); European Research Council, ERC-CoG Mini-HEART 101001746 (M.B.); and EU's H2020 research and innovation programme under Marie Skłodowska-Curie cofund RESCUE grant, 801540 (E.v.R.). **Author contributions:** H.T. performed all molecular biology experiments related to the animal studies and human studies and maintained the mouse colony. S.J.v.K. performed the CRISPR-Cas9 targeting experiments for the animal model and the hiPSC model. S.J.v.K., S.J.H., and J.M.-K. maintained the hiPSC lines and performed the experiments on hiPSC-CMs. V.M., M.B., and C.L.M. were involved with MT experiments. W.B.v.H., S.C., A.B., G.A.M., C.A.R., and T.A.B.v.V. were involved with electrophysiology experiments. A.V. and P.v.d.K. supplied patient tissue samples and performed histological staining on human samples. M.M. and X.Y. performed the global proteomics analysis. J.E. performed the bulk RNA sequencing analyses. D.V. performed the echocardiology measurements on animals and maintained the mouse colony. L.W.v.L. and J.G. provided us with human clinical data. S.J.K. and G.J.P.L.K. performed the karyotyping experiments. H.d.R. performed the molecular experiments. J.A.A.D. and K.B. performed the ubiquitin proteomics analysis. H.T., S.J.v.K., and E.v.R. planned all experiments and wrote the manuscript. **Competing interests:** E.v.R. is a consultant for Tenaya Therapeutics and Novo Nordisk and is Chief Scientific Officer of Phlox Therapeutics. All other authors declare that they have no competing interests. **Data and materials availability:** All data associated with this study are present in the paper or the Supplementary Materials. The bulk RNA sequencing datasets have been deposited with the Gene Expression Omnibus repository (GEO) under accession numbers GSE199925 (animal study) and GSE160289 (hiPSC-CM study). The mass spectrometry proteomics datasets have been deposited in the ProteomeXchange Consortium via the PRIDE partner repository with the dataset identifier PXD020605 (global proteomics analysis) and PXD032964 (ubiquitination diglycine remnant containing peptides proteomics analysis). All submitted datasets are listed under the project name "Desmosomal protein degradation as underlying cause of arrhythmogenic cardiomyopathy." The hiPSC lines are available from M.B. by material transfer agreement with Leiden University Medical Center. Additional details and materials can be made available from the corresponding authors on reasonable request.

Submitted 13 June 2022
Resubmitted 14 December 2022
Accepted 1 March 2023
Published 22 March 2023
10.1126/scitranslmed.add4248

Science Translational Medicine

Desmosomal protein degradation as an underlying cause of arrhythmogenic cardiomyopathy

Hoyee Tsui, Sebastiaan Johannes van Kampen, Su Ji Han, Viviana Meraviglia, Willem B. van Ham, Simona Casini, Petra van der Kraak, Aryan Vink, Xiaoke Yin, Manuel Mayr, Alexandre Bossu, Gerard A. Marchal, Jantine Monshouwer-Kloots, Joep Eding, Danielle Versteeg, Hesther de Ruiter, Karel Bezstarosti, Judith Groeneweg, Sjoerd J. Klaasen, Linda W. van Laake, Jeroen A.A. Demmers, Geert J.P.L. Kops, Christine L. Mummery, Toon A.B. van Veen, Carol Ann Remme, Milena Bellin, and Eva van Rooij

Sci. Transl. Med., **15** (688), eadd4248.
DOI: 10.1126/scitranslmed.add4248